Inorganic Chemistry
Article

Inorg. Chem. **2010**, *49*, 271–284 **271**
DOI: 10.1021/ic901999e

Fluoride Ion Donor Properties of *cis*-OsO_2F_4: Synthesis, Raman Spectroscopic Study, and X-ray Crystal Structure of $[OsO_2F_3][Sb_2F_{11}]$

Michael J. Hughes, Hélène P. A. Mercier, and Gary J. Schrobilgen*

Department of Chemistry, McMaster University, Hamilton, Ontario, L8S 4M1, Canada

Received October 8, 2009

The salt, $[OsO_2F_3][Sb_2F_{11}]$, has been synthesized by dissolution of *cis*-OsO_2F_4 in liquid SbF_5, followed by removal of excess SbF_5 at 0 °C to yield orange, crystalline $[OsO_2F_3][Sb_2F_{11}]$. The X-ray crystal structure (−173 °C) consists of an $OsO_2F_3^+$ cation fluorine bridged to an $Sb_2F_{11}^-$ anion. The light atoms of $OsO_2F_3^+$ and the bridging fluorine atom form a distorted octahedron around osmium in which the osmium atom is displaced from its center toward an oxygen atom and away from the *trans*-fluorine bridge atom. As in other transition metal dioxofluorides, the oxygen ligands are cis to one another and the fluorine bridge atom is trans to an oxygen ligand and cis to the remaining oxygen ligand. The Raman spectrum (−150 °C) of solid $[OsO_2F_3][Sb_2F_{11}]$ was assigned on the basis of the ion pair observed in the low-temperature crystal structure. Under dynamic vacuum, $[OsO_2F_3][Sb_2F_{11}]$ loses SbF_5, yielding the known $[\mu\text{-}F(OsO_2F_3)_2][Sb_2F_{11}]$ salt with no evidence for $[OsO_2F_3][SbF_6]$ formation. Attempts to synthesize $[OsO_2F_3][SbF_6]$ by the reaction of $[OsO_2F_3][Sb_2F_{11}]$ with an equimolar amount of *cis*-OsO_2F_4 or by a 1:1 stoichiometric reaction of *cis*-OsO_2F_4 with SbF_5 in anhydrous HF yielded only $[\mu\text{-}F(OsO_2F_3)_2][Sb_2F_{11}]$. Quantum-chemical calculations at the SVWN and B3LYP levels of theory and natural bond orbital analyses were used to calculate the gas-phase geometries, vibrational frequencies, natural population analysis charges, bond orders, and valencies of $OsO_2F_3^+$, $[OsO_2F_3][Sb_2F_{11}]$, $[OsO_2F_3][SbF_6]$, and $Sb_2F_{11}^-$. The relative thermochemical stabilities of $[OsO_2F_3][SbF_6]$, $[OsO_2F_3][Sb_2F_{11}]$, $[OsO_2F_3][AsF_6]$, $[\mu\text{-}F(OsO_2F_3)_2][SbF_6]$, $[\mu\text{-}F(OsO_2F_3)_2][Sb_2F_{11}]$, and $[\mu\text{-}F(OsO_2F_3)_2][AsF_6]$ were assessed using the appropriate Born−Haber cycles to account for the preference for $[\mu\text{-}F(OsO_2F_3)_2][Sb_2F_{11}]$ formation over $[OsO_2F_3][SbF_6]$ formation and for the inability to synthesize $[OsO_2F_3][SbF_6]$.

Introduction

Relatively few high-valent transition metal oxide fluoride cations are known. For example, the only group 7 oxide fluoride cations that have been structurally characterized are MOF_4^+,[1,2] μ-$F(MOF_4)_2^+$,[1,2] and $MO_2F_2^+$ [3,4] (M = Re, Tc). Examples of oxide fluoride cations of Os(VIII) are also sparse, with only OsO_3F^+ [5] and μ-F(*cis*-$OsO_2F_3)_2^+$ [6] having been fully structurally characterized.

The OsO_3F^+ cation has been characterized in its $[OsO_3F][PnF_6]$ (Pn = As, Sb), $[OsO_3F][HF]_2[AsF_6]$, $[OsO_3F][HF][SbF_6]$, and $[OsO_3F][Sb_3F_{16}]$ salts by low-temperature Raman spectroscopy and single-crystal X-ray diffraction.[5] The PnF_6^- salts contain OsO_3F^+ cations that strongly interact with the anion by means of fluorine bridges and/or coordinate HF to osmium through fluorine to give six-coordinate osmium. In contrast, the disordered OsO_3F^+ cation of $[OsO_3F][Sb_3F_{16}]$, with an osmium coordination number of four, is well isolated from the weakly fluoro-basic $Sb_3F_{16}^-$ anion.

The μ-F(*cis*-$OsO_2F_3)_2^+$ cation has been synthesized by the reaction of *cis*-OsO_2F_4 with either SbF_5 or AsF_5 in anhydrous HF (aHF) solvent and by reaction of *cis*-OsO_2F_4 with liquid AsF_5 and has been isolated as the $Sb_2F_{11}^-$ and AsF_6^- salts.[6] The crystal structure of $[\mu\text{-}F(cis\text{-}OsO_2F_3)_2][Sb_2F_{11}]$ reveals that the cation consists of two symmetry-related $OsO_2F_3^+$ units that are fluorine-bridged to one another. The osmium atoms are six-coordinate, with the oxygen ligands of each osmium atom cis to one another and the fluorine bridge atom trans to two oxygen ligands.

The $OsO_2F_3^+$ cation has been generated in solution by dissolution of *cis*-OsO_2F_4 in liquid SbF_5 and was characterized by ^{19}F NMR and Raman spectroscopy in SbF_5 solutions but was not isolated and structurally characterized in the solid state.[6] The doublet and triplet coupling patterns resulting from $^2J(^{19}F-^{19}F)$ coupling in the ^{19}F NMR spectrum are consistent with a trigonal bipyramidal cation

*To whom correspondence should be addressed. E-mail: schrobil@mcmaster.ca.

(1) Schrobilgen, G. J.; Holloway, J. H.; Russell, D. R. *J. Chem. Soc., Dalton Trans.* **1984**, 1411–1415.
(2) LeBlond, N.; Mercier, H. P. A.; Dixon, D. A.; Schrobilgen, G. J. *Inorg. Chem.* **2000**, *39*, 4494–4509.
(3) Supel, J.; Abram, U.; Hagenbach, A.; Seppelt, K. *Inorg. Chem.* **2007**, *46*, 5591–5595.
(4) LeBlond, N.; Dixon, D. A.; Schrobilgen, G. J. *Inorg. Chem.* **2000**, *39*, 2473–2487.
(5) Gerken, M.; Dixon, D. A.; Schrobilgen, G. J. *Inorg. Chem.* **2002**, *41*, 259–277.
(6) Casteel, W. J.; Dixon, D. A.; Mercier, H. P. A.; Schrobilgen, G. J. *Inorg. Chem.* **1996**, *35*, 4310–4322.

Published on Web 12/01/2009

geometry in which the oxygen atoms and a fluorine atom are in equatorial positions and two fluorine atoms are in axial positions. The polymeric $Sb_nF_{5n+1}^-$ anions generated upon ionization of *cis*-OsO_2F_4 in this medium are expected to be very weakly fluoro-basic and to weakly interact with the cation by means of fluorine bridges. The fluorine bridge environments and their attendant couplings to the fluorine resonances of $OsO_2F_3^+$, however, were not observed in the prior NMR study[6] and are therefore presumed to be labile on the ^{19}F NMR time scale. The Raman spectrum of $OsO_2F_3^+$ in SbF_5 solvent was assigned under C_{2v} symmetry on the basis of the ^{19}F NMR spectrum and the calculated frequencies for the energy-minimized gas-phase trigonal bipyramidal geometry.[6]

In the current study, the first $OsO_2F_3^+$ salt has been isolated and structurally characterized by single-crystal X-ray diffraction and low-temperature Raman spectroscopy. The thermochemistries of the reactions of *cis*-OsO_2F_4 with PnF_5 (Pn = As, Sb) have also been investigated in the gas phase and in the solid state.

Results and Discussion

Synthesis of $[OsO_2F_3][Sb_2F_{11}]$ and Attempted Synthesis of $[OsO_2F_3][SbF_6]$. The salt, $[OsO_2F_3][Sb_2F_{11}]$, was synthesized by the dissolution of *cis*-OsO_2F_4 in liquid SbF_5 (eq 1).

$$cis\text{-}OsO_2F_4 + 2SbF_5 \xrightarrow[25\ ^\circ C]{SbF_5} [OsO_2F_3][Sb_2F_{11}] \quad (1)$$

Polycrystalline samples of the salt and single crystals suitable for X-ray structure determination were isolated by slow removal of the SbF_5 solvent under dynamic vacuum at 0 °C, yielding deep orange $[OsO_2F_3][Sb_2F_{11}]$ in nearly quantitative yield.

In an attempt to isolate $[OsO_2F_3][SbF_6]$, the $[OsO_2F_3][Sb_2F_{11}]$ salt was pumped under vacuum to remove SbF_5, according to eq 2. Monitoring of the sample composition by Raman spectroscopy at intervals during pumping revealed that the only species present were $[OsO_2F_3][Sb_2F_{11}]$ and $[\mu\text{-}F(OsO_2F_3)_2][Sb_2F_{11}]$, at constant sample mass, the only species remaining was $[\mu\text{-}F(OsO_2F_3)_2][Sb_2F_{11}]$ (eq 3).[6]

$$[OsO_2F_3][Sb_2F_{11}] \xrightarrow[0\ ^\circ C]{vac} [OsO_2F_3][SbF_6] + SbF_5 \quad (2)$$

$$2[OsO_2F_3][Sb_2F_{11}] \xrightarrow[0\ ^\circ C]{vac} [\mu\text{-}F(OsO_2F_3)_2][Sb_2F_{11}] + 2SbF_5 \quad (3)$$

In other attempts to isolate $[OsO_2F_3][SbF_6]$, (1) *cis*-OsO_2F_4 was dissolved in aHF containing a 10-fold excess of SbF_5 with respect to the $OsO_2F_3^+$ cation. Anhydrous HF solvent was used to favor the more fluoro-basic SbF_6^- anion and the formation of $[OsO_2F_3][SbF_6]$. Again, Raman spectroscopy confirmed that only $[\mu\text{-}F(OsO_2F_3)_2][Sb_2F_{11}]$ was isolated (eq 4). (2) A mixture of *cis*-OsO_2F_4 and $[OsO_2F_3][Sb_2F_{11}]$ in a 2:1 molar ratio was allowed to react in aHF at 25 °C. Raman spectroscopy revealed that only $[\mu\text{-}F(OsO_2F_3)_2][Sb_2F_{11}]$ had formed in admixture with *cis*-OsO_2F_4 when HF was removed under dynamic vacuum at −78 °C (eq 5). Fusion of the resulting mixture at 90 °C for 1 h also did not result in further reaction.

$$2cis\text{-}OsO_2F_4 + 2SbF_5 \xrightarrow[25\ ^\circ C]{HF/SbF_5} [\mu\text{-}F(OsO_2F_3)_2][Sb_2F_{11}] \quad (4)$$

$$2cis\text{-}OsO_2F_4 + [OsO_2F_3][Sb_2F_{11}] \xrightarrow[-78\ ^\circ C]{HF} [\mu\text{-}F(OsO_2F_3)_2][Sb_2F_{11}] + cis\text{-}OsO_2F_4 \quad (5)$$

Table 1. Summary of Crystal Data and Refinement Results for $[OsO_2F_3][Sb_2F_{11}]$

chem formula	$OsO_2F_{14}Sb_2$
space group	$P\bar{1}$ (no. 2)
a (Å)	7.4284(3)
b (Å)	8.6649(4)
c (Å)	10.0394(4)
α (deg)	97.597(2)
β (deg)	111.263(2)
γ (deg)	110.697(2)
V (Å^3)	537.39(4)
molecules/unit cell	2
mol wt (g mol^{-1})	1463.40
calcd density (g cm^{-3})	4.522
T (°C)	−173
μ (mm^{-1})	16.98
R_1[a]	0.0426
wR_2[b]	0.0694

[a] R_1 is defined as $\sum||F_o| - |F_c||/\sum|F_o|$ for $I > 2\sigma(I)$. [b] wR_2 is defined as $\{\sum[w(F_o^2 - F_c^2)^2]/\sum w(F_o^2)^2\}^{1/2}$ for $I > 2\sigma(I)$.

X-ray Crystal Structure of $[OsO_2F_3][Sb_2F_{11}]$. Details of data collection parameters and other crystallographic information are provided in Table 1, and geometric parameters are listed in Table 2. The crystal structure consists of discrete $[OsO_2F_3][Sb_2F_{11}]$ ion pairs (Figure 1a) that are well isolated from one another. There is a short contact (2.190(3) Å) between the osmium atom and a terminal fluorine atom, F(4), cis to the Sb(1)---F(9)---Sb(2) bridge of the $Sb_2F_{11}^-$ anion. Such *cis*-fluorine bridge arrangements have been observed for other $Sb_2F_{11}^-$ salts, for example, $[XeF_3][Sb_2F_{11}]$,[7] $[XeF][Sb_2F_{11}]$,[8] $[XeF(HF)][Sb_2F_{11}]$,[9] $[BrF_4][Sb_2F_{11}]$,[10] $[(F_3As)AuXe][Sb_2F_{11}]$,[11] and $[N_5][Sb_2F_{11}]$.[12] The two bridging fluorine atoms of the $[OsO_2F_3][Sb_2F_{11}]$ ion pair, F(4) and F(9), lay only 0.121 and 0.072 Å, respectively, out of the [Sb(1), Sb(2), Os]-plane.

The $[OsO_2F_3][Sb_2F_{11}]$ ion pairs are stacked, without alternation, along the *c*-axis but alternate along the *a*- and *b*-axes (Figure S1) so that the anions and cations of different ion pairs face one another in columns that run parallel to these axes. The resulting F···F and O···F contacts between nearest-neighbor ion pairs are long

(7) McKee, D. E.; Zalkin, A.; Bartlett, N. *Inorg. Chem.* **1973**, *12*, 1713–1717.
(8) McRae, V. M.; Peacock, R. D.; Russell, D. R. *J. Chem. Soc. D* **1969**, 62–63.
(9) Drews, T.; Seppelt, K. *Angew. Chem., Int. Ed. Engl.* **1997**, *36*, 273–274.
(10) Lind, M. D.; Christe, K. O. *Inorg. Chem.* **1972**, *11*, 608–612.
(11) Hwang, I.-C.; Seidel, S.; Seppelt, K. *Angew. Chem., Int. Ed. Engl.* **2003**, *42*, 4392–4395.
(12) Vij, A.; Wilson, W. W.; Vij, V.; Tham, F. S.; Sheehy, J. A.; Christe, K. O. *J. Am. Chem. Soc.* **2001**, *123*, 6308–6313.
(13) Bondi, A. *J. Phys. Chem.* **1964**, *68*, 441–451.
(14) The long contacts within the sum of the van der Waals radii in $[OsO_2F_3][Sb_2F_{11}]$ are F(1)···F(1A) (2.659(7) Å), F(1)···F(8B) (2.727(5) Å), F(1)···F(5A) (2.769(5) Å), O(2)···F(7C) (2.763(5) Å), F(7)···F(7C) (2.771(7) Å), F(8)···F(8B) (2.801(8) Å), and O(2)···F(10D) (2.808(4) Å), The corresponding sums of the van der Waals radii (taken from ref 13) are F···F (2.694 Å) and O···F (2.699 Å).

Table 2. Experimental Geometrical Parameters for $[OsO_2F_3][Sb_2F_{11}]$ and Calculated Geometrical Parameters for $[OsO_2F_3][Sb_2F_{11}]$, $OsO_2F_3^+$, and $Sb_2F_{11}^-$

	exptl[a]	calcd					
	$[OsO_2F_3][Sb_2F_{11}]$	$[OsO_2F_3][Sb_2F_{11}]$ (C_1)		$OsO_2F_3^+$ (C_{2v})		$Sb_2F_{11}^-$ (C_1)	
		SVWN[b]	B3LYP[c]	SVWN[b]	B3LYP[c]	SVWN[b]	B3LYP[d]
				Bond Lengths (Å)			
Os−F(1)	1.812(4)	1.870	1.862	1.836	1.828		
Os−F(2)	1.791(3)	1.835	1.826	1.828	1.824		
Os−F(3)	1.806(3)	1.852	1.843	1.828	1.824		
Os−O(1)	1.654(4)	1.696	1.670	1.689	1.663		
Os−O(2)	1.764(4)	1.708	1.677	1.689	1.663		
Os---F(4)	2.190(3)	2.089	2.086				
Sb(1)−F(4)	1.958(3)	2.085	2.104			1.909	1.895
Sb(1)−F(5)	1.851(3)	1.892	1.876			1.904	1.895
Sb(1)−F(6)	1.836(3)	1.879	1.866			1.902	1.896
Sb(1)−F(7)	1.844(3)	1.881	1.872			1.908	1.896
Sb(1)−F(8)	1.837(3)	1.884	1.878			1.906	1.898
Sb(1)---F(9)	1.995(3)	2.027	1.992			2.080	2.076
Sb(2)---F(9)	2.060(3)	2.139	2.197			2.080	2.076
Sb(2)−F(10)	1.862(3)	1.884	1.874			1.906	1.898
Sb(2)−F(11)	1.848(4)	1.892	1.877			1.909	1.896
Sb(2)−F(12)	1.856(4)	1.890	1.882			1.908	1.894
Sb(2)−F(13)	1.844(3)	1.935	1.907			1.904	1.896
Sb(2)−F(14)	1.855(4)	1.903	1.890			1.902	1.894
				Bond Angles (deg)			
O(1)−Os−O(2)	99.9(2)	103.1	102.3	108.6	108.7		
O(1)−Os−F(1)	100.1(2)	97.6	96.6	125.7	125.7		
O(1)−Os−F(2)	100.2(2)	96.6	96.8	95.5	95.4		
O(1)−Os−F(3)	100.1(2)	100.1	97.6	95.5	95.4		
O(1)−Os---F(4)	179.2(2)	173.7	175.0				
O(2)−Os−F(1)	159.9(2)	158.5	160.9	125.7	125.7		
O(2)−Os−F(2)	90.3(2)	96.1	95.8	95.5	95.4		
O(2)−Os−F(3)	88.6(2)	89.9	92.4	95.5	95.4		
O(2)−Os---F(4)	80.9(2)	81.8	82.6				
F(1)−Os−F(2)	87.8(2)	87.0	84.5	80.6	80.7		
F(1)−Os−F(3)	86.2(2)	80.8	82.4	80.6	80.7		
F(1)−Os---F(4)	79.1(1)	78.0	78.5				
F(2)−Os−F(3)	159.6(2)	160.4	161.6	164.6	161.4		
F(2)−Os---F(4)	79.5(1)	78.8	82.2				
F(3)−Os---F(4)	80.2(1)	83.7	82.5				
Os---F(4)−Sb(1)	173.0(2)	135.8	154.4				
F(4)−Sb(1)−F(5)	86.6(2)	83.3	84.1			89.3	89.9
F(4)−Sb(1)−F(6)	171.5(1)	175.3	175.5			170.0	172.4
F(4)−Sb(1)−F(7)	87.1(2)	81.6	82.8			88.9	89.6
F(4)−Sb(1)−F(8)	90.9(1)	85.9	86.4			94.7	93.8
F(4)−Sb(1)---F(9)	83.4(1)	86.1	84.4			83.9	86.3
F(5)−Sb(1)−F(6)	92.0(2)	96.6	96.2			90.6	89.9
F(5)−Sb(1)−F(7)	168.6(2)	161.1	165.3			171.2	172.2
F(5)−Sb(1)−F(8)	94.7(2)	94.3	92.6			94.5	94.0
F(5)−Sb(1)---F(9)	84.5(1)	81.5	86.1			86.3	87.0
F(6)−Sb(1)−F(7)	92.9(2)	97.5	96.3			89.7	89.6
F(6)−Sb(1)−F(8)	97.6(2)	98.8	98.0			95.3	93.8
F(6)−Sb(1)---F(9)	88.0(1)	89.2	91.2			86.1	86.1
F(7)−Sb(1)−F(8)	94.9(1)	95.9	93.1			94.2	93.8
F(7)−Sb(1)---F(9)	85.3(1)	86.1	86.1			85.0	85.3
F(8)−Sb(1)---F(9)	174.3(2)	171.0	170.8			179.2	179.1
Sb(1)---F(9)---Sb(2)	170.0(2)	142.0	158.2			133.7	161.5
F(9)---Sb(2)−F(10)	178.5(2)	176.0	178.5			178.4	179.1
F(9)---Sb(2)−F(11)	85.5(1)	84.2	83.3			83.9	85.6
F(9)---Sb(2)−F(12)	85.3(1)	84.2	83.7			85.0	86.8
F(9)---Sb(2)−F(13)	84.4(1)	81.0	82.7			86.3	85.6
F(9)---Sb(2)−F(14)	85.2(1)	81.6	83.6			86.1	86.7
F(10)−Sb(2)−F(11)	94.1(2)	97.4	96.6			94.7	93.8
F(10)−Sb(2)−F(12)	96.2(2)	99.4	97.8			94.2	93.9
F(10)−Sb(2)−F(13)	94.2(2)	95.3	95.8			94.5	93.8
F(10)−Sb(2)−F(14)	95.1(2)	96.4	96.5			95.3	93.8
F(11)−Sb(2)−F(12)	89.4(2)	91.6	90.7			88.9	89.7
F(11)−Sb(2)−F(13)	90.5(2)	87.3	88.9			89.3	89.5
F(11)−Sb(2)−F(14)	170.7(2)	165.3	166.7			170.0	172.4
F(12)−Sb(2)−F(13)	169.7(2)	165.2	166.3			171.3	172.4
F(12)−Sb(2)−F(14)	88.6(2)	90.8	89.8			89.7	90.0
F(13)−Sb(2)−F(14)	89.9(2)	86.7	87.5			90.6	89.7

[a] For the atom labeling scheme, see Figure 1a. [b] The SDDall basis set was used augmented for F, O, and Sb with two d-type polarization functions. [c] The Stuttgart basis set was used for Os with the f functional. The aug-cc-pVTZ basis sets were used for all other atoms. [d] The aug-cc-pVTZ(-PP) basis set was used.

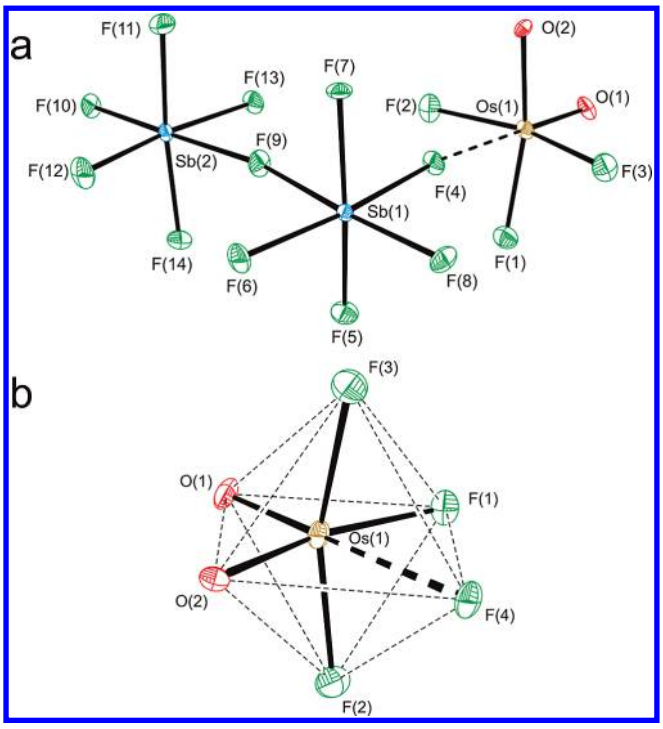

Figure 1. (a) Structural unit in the X-ray crystal structure of [*cis*-OsO_2F_3][Sb_2F_{11}] with thermal ellipsoids drawn at the 70% probability level. (b) Visualization of the octahedron formed by the light atoms of the OsO_2F_4 unit.

and near the sums of the van der Waals radii for oxygen and fluorine.[13,14]

The oxygen atoms of $OsO_2F_3^+$ are cis to one another as found in $(OsO_3F_2)_\infty$,[15] $(OsO_3F_2)_2 \cdot 2XeOF_4$,[16] *cis*-$OsO_2F_4$,[17] and F(*cis*-$OsO_2F_3)_2^+$[6] and in other transition metal oxide fluorides such as $MoO_2F_2 \cdot 2THF$ (THF = tetrahydrofuran),[18] *cis*-$TcO_2F_4^-$,[19] TcO_2F_3,[4] ReO_2F_3,[20] *cis*-$ReO_2F_4^-$,[20] μ-F(*cis*-$ReO_2F_3)_2^-$,[20] and $Re_3O_6F_{10}^-$.[20] The *cis*-dioxo geometry may be accounted for in terms of the relative spatial orientations of the approximate $d_{t_{2g}}$ orbitals of the d^0 metal and the availability of filled oxygen p donor orbitals.[21]

The lengths of the Os−O(1) bond trans to the bridging fluorine atom (1.654(4) Å) and the Os−O(2) bond trans to a terminal fluorine atom (1.764(4) Å) are comparable to those found in μ-F$(OsO_2F_3)_2^+$ (1.65(1) and 1.73(1) Å, respectively)[6] and $(OsO_3F_2)_\infty$ (1.69(1)/1.68(1) and 1.73(1) Å, respectively).[15] The terminal Os−F(1,2,3) bond lengths (1.812(4), 1.791(3), 1.806(3) Å) are also comparable to those in μ-F(*cis*-$OsO_2F_3)_2^+$ (1.79(1), 1.76(1) Å). The Os---F(4) bridge bond (2.190(3) Å) is somewhat longer than the Os---F bridge bonds of $(OsO_3F_2)_\infty$ (2.126(1), 2.108(1) Å),[15] $(OsO_3F_2)_2 \cdot 2XeOF_4$ (2.117(5) Å),[16] and μ-F(*cis*-$OsO_2F_3)_2^+$ (2.086(3) Å)[6] and is consistent with an ion-pair interaction.

The trans position of the bridging fluorine, F(4), results from the trans influence of the doubly bonded oxygen, O(1), which competes more effectively for the osmium $d_{t_{2g}}$ orbitals than F(4). Consequently, the F(4) atom is more strongly bonded to the Sb atom with a bond length of 1.958(3) Å and a negative charge that is less than those of the terminal fluorine ligands bonded to osmium and antimony (see Computational Results). The bond length trend, Os−O(1) < Os−O(2), is also a consequence of less effective competition of the bridging fluorine atom (F(4)) for the empty metal $d_{t_{2g}}$ orbitals than the terminal fluorine atom (F(1)). The tendency for bridging fluorine atoms to occupy positions trans to O atoms has also been noted in other transition metal oxide fluorides and their cations, e. g., μ-F(*cis*-$OsO_2F_3)_2^+$,[6] $(OsO_3F_2)_2 \cdot 2XeOF_4$,[16] $(OsO_3F_2)_\infty$,[15] polymeric $TcO_2F_3 \cdot SbF_5$,[4] $ReO_2F_3 \cdot SbF_5$,[2] μ-F$(TcOF_4)_2^+$,[2] μ-F$(ReOF_4)_2^-$,[1] μ-F(cis-$ReO_2F_3)_2^+$,[20] $Re_3O_6F_{10}^-$,[19] WOF_4,[22] and $MoOF_4$.[22]

Removal of a fluoride ion from *cis*-OsO_2F_4 to form *cis*-$OsO_2F_3^+$ results in contraction of the terminal Os−F bond lengths relative to those of *cis*-OsO_2F_4 (1.883(3) and 1.843(3) Å).[17] This is expected because cation formation results in a higher Os charge and a higher electronegativity for Os, leading to shorter and more covalent Os−F bonds. The length of the Os−O(1) bond trans to the bridging fluorine atom (1.654(4) Å) is comparable to that of *cis*-OsO_2F_4 (1.674(4) Å),[17] while the Os−O(2) bond length trans to the terminal fluorine ligand (1.764(4) Å) is longer than that of *cis*-OsO_2F_4. The longer Os−O(2) bond length likely results from a secondary bonding interaction between O(2) and F(8) of an adjacent $Sb_2F_{11}^-$ anion (O(2)···F(8), 2.808(4) Å).

The light atoms of the $OsO_2F_3^+$ cation and F(4) of the $Sb_2F_{11}^-$ anion comprise a distorted octahedral coordination sphere about osmium (Figure 1b). Although there is significant variation in the bond lengths around the osmium atom, the octahedron formed by the light atoms is relatively undistorted, as shown by the ranges of nearest-neighbor ligand atom contacts.[23] The Os−F(1,2,3) and Os−O(2) bonds are bent away from the Os−O(1) bond, toward the longer Os---F(4) bridge bond. The F(1), F(2), O(2), and F(3) atoms are coplanar within ±0.003 Å, and the bond angles subtended by the Os−O(1) bond and this plane are all very close to 100°. The osmium atom is displaced from the center of the light atom octahedron toward O(1), lying 0.314 Å out of the [F(1), F(2), O(2), F(3)]-plane. In contrast, the Os atom is coplanar, to within ±0.02 Å, with the two remaining orthogonal ligand planes, [O(1), F(2), F(3), F(4)] and [O(1), O(2), F(1), F(4)]. This distortion is consistent with that observed for the μ-F(*cis*-$OsO_2F_3)_2^+$ cation,[6] where

(15) Bougon, R.; Buu, B.; Seppelt, K. *Chem. Ber.* **1993**, *126*, 1331–1336.
(16) Hughes, M. J.; Mercier, H. P. A.; Schrobilgen, G. J. *Inorg. Chem.* **2009**, *48*, 4478–4490.
(17) Christe, K. O.; Dixon, D. A.; Mack, H. G.; Oberhammer, H.; Pagelot, A.; Sanders, J. C. P.; Schrobilgen, G. J. *J. Am. Chem. Soc.* **1993**, *115*, 11279–11284.
(18) Rhiel, M.; Wocadlo, S.; Massa, W.; Dehnicke, K. *Z. Anorg. Allg. Chem.* **1996**, *622*, 1195–1199.
(19) Casteel, W. J.; Dixon, D. A.; LeBlond, N.; Mercier, H. P. A.; Schrobilgen, G. J. *Inorg. Chem.* **1998**, *37*, 340–353.
(20) Casteel, W. J.; Dixon, D. A.; LeBlond, N.; Lock, P. E.; Mercier, H. P. A.; Schrobilgen, G. J. *Inorg. Chem.* **1999**, *38*, 2340–2358.
(21) The *cis*-dioxo geometry has d_{xy}, d_{yz}, and d_{xz} orbitals with correct symmetries for overlap with the p orbitals of oxygen, whereas the *trans*-dioxo geometry has one p orbital per oxygen ligand that has the correct symmetry to compete for a single $d_{t_{2g}}$ orbital on the metal. This causes the orbital energies of the trans isomer to be higher than those of the cis isomer, making the cis isomer more favorable.
(22) Edwards, A. J.; Jones, G. R.; Steventon, B. R. *Chem. Commun.* **1967**, 462–464.
(23) The interatomic distances for the light atoms forming the coordination spheres of the Os atoms in [OsO_2F_3][Sb_2F_{11}] are O(1)···F(1,2,3) 2.659(6), 2.645(5), 2.654(5) Å; O(1)···O(2) 2.618(6) Å; F(4)···F(1,2,3) 2.564(5), 2.564 (5), 2.590(4) Å; F(1)···F(2,3) 2.499(5), 2.473(5) Å; and O(2)···F(2,3) 2.521(5), 2.494(5) Å.

each Os atom is also displaced toward an O atom trans to the fluorine bridge. The out-of-center displacements of the Os atoms of both cations differ from their counterparts in *cis*-OsO_2F_4,[17] *cis*-$ReO_2F_4^-$,[20] and *cis*-$TcO_2F_4^-$,[19] where the metal atom is symmetrically displaced toward both O atoms of the *cis*-MO_2 group, with the orthogonal [O, M, O]- and [F_{ax}, M, F_{ax}]-planes bisecting each other.

The anion−cation close contact results in significant elongation of the Sb(1)−F(4) bridge bond (1.958(3) Å) when compared with the average of the terminal Sb−F bond lengths (1.847(3) Å). Such elongations have been noted for other ion pairs, for example, [XeF][Sb_2F_{11}] (1.93(4), 1.84(4) Å),[8] [XeF_3][Sb_2F_{11}] (1.90(1), 1.85(1) Å),[7] and [$Ir_4(CO)_8$-(μ-F_2)($Sb_2F_{11})_2$] (1.886(3), 1.856(3) Å).[24] The Os---F(4)−Sb bridge angle (173.0(2)°) is slightly bent and compares well with those of [BrF_4][Sb_2F_{11}] (Br---F−Sb (170(5)°)),[10] [XeF_3][Sb_2F_{11}] (Xe---F−Sb (171.6(1)°),[7] and [(F_3As)AuXe]-[Sb_2F_{11}] (Au---F−Sb (173.26(2)°)).[11] The Sb(1)---F(9)---Sb(2) bond angle is also slightly bent (170.0(2)°). Both bridge angles are in good agreement with the fluorine bridge angles of other cubic close-packed structures such as WOF_4 (173(1)°),[25] [SeF_3][NbF_6] (173(3), 171(6), 176(8), 176(4)°),[26] [SeF_3][Nb_2F_{11}] (166(2), 177(1), 167(2), 170(2)°),[27] and [NbF_4][SbF_6] (162.9(8), 164.0(8)°).[28]

The $Sb_2F_{11}^-$ anion has a nearly eclipsed conformation, with a dihedral angle, ψ, between the SbF_4 equatorial planes of the SbF_5 units that share the fluorine bridge atom of 6.9° for F(5,7,8,9) and F(9,10,11,14) and 5.3° for F(4,6,8,9) and F(9,10,12,13). The correlation between the M---F---M bridge angle of a $M_2F_{11}^-$ anion and ψ is well-documented,[10] and results from minimization of the steric repulsions between the nearest neighbor fluorine atoms of each octahedron as the M---F---M angle decreases and ψ increases. Accordingly, ψ is 0° when the M---F---M is 180°, reaching a maximum of 45° when M---F---M is ca. 145°.

Raman Spectroscopy. The solution Raman spectrum of *cis*-OsO_2F_4 in liquid SbF_5 has been previously assigned on the basis of a trigonal bipyramidal geometry for the $OsO_2F_3^+$ cation and polymeric $Sb_nF_{5n+1}^-$ anions.[6] The low-temperature solid-state Raman spectrum of [OsO_2F_3][Sb_2F_{11}] has been obtained in the present study (Figure 2). The higher spectral resolution, knowledge of the X-ray crystal structure, and a factor-group analysis have enabled the complete vibrational assignment of the [OsO_2F_3][Sb_2F_{11}] ion pair.

The observed and calculated frequencies and their assignments are listed in Table 3. The spectral assignments for [OsO_2F_3][Sb_2F_{11}] were made by comparison with calculated frequencies and Raman intensities of the gas-phase [OsO_2F_3][Sb_2F_{11}] ion pair, $Sb_2F_{11}^-$ (Table 3), and the [OsO_2F_3][SbF_6] ion pair (Table S1), which are in good agreement at the SVWN/SDDall(-PP) and B3LYP/aug-cc-pVTZ(-PP) levels of theory.

The calculated $Sb_2F_{11}^-$ frequencies show better agreement with the experimental values than those previously calculated at the B3LYP/3-21G* level.[29,30] The previous calculations overestimated the Sb−F stretching frequencies by ca. 70 cm^{-1}, whereas the frequencies calculated in the current study are overestimated by ca. 30 cm^{-1}.

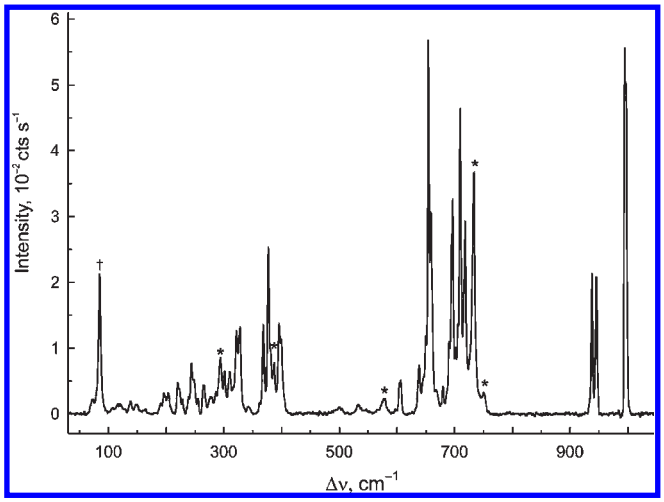

Figure 2. Raman spectrum of [OsO_2F_3][Sb_2F_{11}] recorded at −150 °C using 1064-nm excitation. The symbols denote FEP sample tube lines (∗) and an instrumental artifact (†).

The vibrational modes (51 A) of the [OsO_2F_3][Sb_2F_{11}] ion pair corresponding to the gas-phase energy-minimized symmetry, C_1, are all predicted to be Raman- and infrared-active. It is apparent from Table 3 that the majority of the bands are split into two components. Consequently, a factor-group analysis was undertaken on the basis of the crystal structure determination (see X-ray Crystal Structure of [OsO_2F_3][Sb_2F_{11}]). The analysis (Table S2) correlated the gas-phase symmetry of the ion pair (C_1) to its site symmetry (C_1), which, in turn, was correlated to the unit cell symmetry (C_i). The factor-group analysis, however, revealed that the Raman bands of [OsO_2F_3][Sb_2F_{11}] are not expected to be split. X-ray powder diffraction patterns (Figure S2) recorded on the same sample confirmed that a single phase was present between the temperature at which the Raman spectrum was recorded (−150 °C) and the temperature at which the single-crystal X-ray data were collected (−173 °C). Moreover, the powder patterns recorded at −150 and −173 °C were in agreement with the powder pattern calculated from the single-crystal data. It may be concluded that the splitting does not arise from a phase transition in this temperature range. In addition to the centrosymmetric space group, $P\bar{1}$, the structure was solved in the $P1$ space group, which could account for the splittings in the Raman spectrum (Table S2); however, the refinement in this space group proved to be unstable, with the thermal parameters of many light atoms becoming nonpositive when attempting to refine them anisotropically. Presently, the splittings of the Raman bands cannot be accounted for unless the unit cell is not truly centrosymmetric and the vibrational spectrum better represents the true symmetry. Such a situation is illustrated by [$H_3O\cdot 2XeF_2$][AsF_6].[31]

(24) Hwang, I.-C.; Seppelt, K. *Inorg. Chem.* **2003**, *42*, 7116–7122.
(25) Edwards, A. J.; Jones, G. R. *J. Chem. Soc. A* **1968**, 2074–2078.
(26) Edwards, A. J.; Jones, G. R. *J. Chem. Soc. A* **1970**, 1891–1894.
(27) Edwards, A. J.; Jones, G. R. *J. Chem. Soc. A* **1970**, 1491–1497.
(28) Edwards, A. J. *J. Chem. Soc., Dalton Trans.* **1972**, 2325–2328.
(29) Sham, I. H. T.; Patrick, B. O.; von Ahsen, B.; von Ahsen, S.; Willner, H.; Thompson, R. C.; Aubke, F. *Solid State Sci.* **2002**, *4*, 1457–1463.
(30) Ahsen, B.; Bach, C.; Berkei, M.; Kockerling, M.; Willner, H.; Hagele, G.; Aubke, F. *Inorg. Chem.* **2003**, *42*, 3801–3814.
(31) Gerken, M.; Moran, M. D.; Mercier, H. P. A.; Pointner, B. E.; Schrobilgen, G. J.; Hoge, B.; Christe, K. O.; Boatz, J. A. *J. Am. Chem. Soc.* **2009**, *131*, 13474–13489.

Table 3. Raman Frequencies, Intensities, and Assignments for $[OsO_2F_3][Sb_2F_{11}]$ and Calculated Vibrational Frequencies and Assignments for $[OsO_2F_3][Sb_2F_{11}]$ and $Sb_2F_{11}^-$

$[OsO_2F_3][Sb_2F_{11}]$	$[OsO_2F_3][Sb_2F_{11}]$ (C_1)			$Sb_2F_{11}^-$ (C_1)		
exptl[a]	calcd[b]		assgnts[c,d]	calcd[b]		assgnts[c,e]
	SVWN[f]	B3LYP[g]		SVWN[f]	B3LYP[h]	
997(89), 995(99)	1006(70)[71]	1055(76)[63]	$\nu(OsO_1) + \nu(OsO_2)$			
946(37), 938(37)	973(79)[25]	1024(25)[64]	$\nu(OsO_1) - \nu(OsO_2)$			
718(52), 716 sh	734(32)[91]	732(7)[158]	$\nu(OsF_2) - \nu(OsF_3)$			
709(82), 706(24) 702(18)	710(108)[64]	710(28)[101]	$\nu(OsF_1) + \nu(OsF_2) + \nu(OsF_3)$			
696(58), 695 sh	695(19)[93]	712(1)[96]	$\nu(SbF_5) - \nu(SbF_7)$	666(<0.1)[195]	675(<0.1)[259]	$[\nu(SbF_5) - \nu(SbF_7)] + [\nu(Sb'F_{14}) - \nu(Sb'F_{11})]$
691(19), 686 sh	677(12)[132]	700(6)[134]	$\nu(SbF_6)$	665(<1)[236]	675(<0.1)[266]	$[\nu(SbF_6) - \nu(SbF_4)] + [\nu(Sb'F_{14}) - \nu(Sb'F_{11})] + [\nu(Sb'F_{13}) - \nu(Sb'F_{12})]$
680(7)	672(21)[39]	695(1)[58]	$\nu(Sb'F_{11}) - \nu(Sb'F_{14})$	655(<1)[25]	667(<0.1)[8]	$[\nu(SbF_5) - \nu(SbF_7)] + [\nu(Sb'F_{11}) - \nu(Sb'F_{14})]$
669(6)	664(14)[59]	685(15)[42]	$\nu(SbF_8) + \nu(Sb'F_{10})$	655(<1)[24]	667(<0.1)[<1]	$[\nu(SbF_4) - \nu(SbF_6)] + [\nu(Sb'F_{13}) - \nu(Sb'F_{12})]$
659(54), 654(100)	668(14)[41]	676(4)[86]	$\nu(Sb'F_{12}) - \nu(Sb'F_{13})$	632(19)[26]	641(29)[3]	$\nu(SbF_8) + \nu(Sb'F_{10})$
649(21), 646(10)	657(3)[172]	673(2)[154]	$\nu(SbF_8) - \nu(Sb'F_{10})$	625(2)[191]	632(<1)[166]	$\nu(SbF_8) - \nu(Sb'F_{10})$
638(13)	660(12)[22]	651(7)[28]	$\nu(OsF_1) - [\nu(OsF_2) + \nu(OsF_3)]$			
608(7), 604(8)	628(23)[16]	640(8)[34]	$\nu(SbF_5) + \nu(SbF_4) + \nu(SbF_9)$	614(<1)[1]	622(<1)[92]	$[\nu(SbF_4) + \nu(SbF_5) + \nu(SbF_6) + \nu(SbF_7) + \nu(SbF_9)] - [\nu(Sb'F_{11} + \nu(Sb'F_{12}) + \nu(Sb'F_{13}) + \nu(Sb'F_{14}) + \nu(Sb'F_9)]$
578(4)	617(54)[37]	632(38)[28]	$\nu(Sb'F_{11}) + \nu(Sb'F_{14})$	611(56)[8]	615(38)[2]	$[\nu(SbF_4) + \nu(SbF_5) + \nu(SbF_6) + \nu(SbF_7)] + [\nu(Sb'F_{11}) + \nu(Sb'F_{12}) + \nu(Sb'F_{13}) + \nu(Sb'F_{14})]$
n.o.	562(12)[74]	578(20)[23]	$[\nu(Sb'F_{12}) + \nu(Sb'F_{13})] - [\nu(Sb'F_{11}) + \nu(Sb'F_{14})]$	584(4)[2]	578(3)[<1]	$[\nu(SbF_4) + \nu(SbF_6)] - [\nu(SbF_5) + \nu(SbF_7)] + [\nu(Sb'F_{12}) + \nu(Sb'F_{13})] - [\nu(Sb'F_{11}) + \nu(Sb'F_{14})]$
533(2)	504(9)[132]	511(10)[154]	$[\nu(OsF_4) - \nu(SbF_4)] + [\nu(Sb'F_9) - \nu(SbF_9)]$	583(3)[1]	578(3)[<1]	$[\nu(SbF_4) + \nu(SbF_6)] - [\nu(SbF_5) + \nu(SbF_7)] + [\nu(Sb'F_{11}) + \nu(Sb'F_{14})] - [\nu(Sb'F_{12}) + \nu(Sb'F_{13})]$
500(1)	475(32)[40]	466(2)[109]	$[\nu(OsF_4) - \nu(SbF_4)] - [\nu(Sb'F_9) - \nu(SbF_9)]$	475(<1)[135]	473(<0.1)[168]	$\nu(SbF_9) - \nu(Sb'F_9)$
n.o.	385(14)[8]	410(8)[15]	$\delta(O_1OsO_2)$			
399(20), 396(24)	358(3)[3]	375(6)[1]	$\delta(O_2OsF_2) + \delta(F_1OsF_3)$			
380 sh, 377(45)	367(5)[17]	339(4)[5]	$\delta(O_1OsF_2) + \delta(F_3OsF_9)$			
368(24), 362(2)	315(4)[3]	332(3)[16]	$\delta(F_1OsF_4) + \rho_w(F_2OsF_3)$			
343(1)	324(3)[20]	304(2)[1]	$\delta_{umb}(OsO_2F_1F_2F_3) + \rho_r(O_1OsF_4) + \delta_{umb}(SbF_4F_5F_8F_9)$			
317 sh, 310(11), 302(11)	302(8)[1]	300(1)[35]	$[OsO_2F_3][Sb_2F_{11}]$ coupled def.	347(3)[31]	298(<1)[27]	$\nu(SbF_9) + \nu(Sb'F_9)$
286(6)	286(2)[12]	290(1)[55]	$\delta(F_{13}Sb'F_{14}) - \delta(F_7SbF_9)$			
276(4) br	265(3)[42]	287(1)[11]	$\delta(F_{12}Sb'F_{14}) + \delta(F_9Sb'F_{11}) - \delta(F_9SbF_7)$	272(<1)[<0.1]	284(<0.1)[40]	$\delta(SbF_9Sb') + \delta_{umb}(SbF_{4,6,7,8}) + \delta_{umb}(Sb'F_{11,12,13,14})$
n.o.	253(8)[13]	280(<1)[5]	$[OsO_2F_3][Sb_2F_{11}]$ coupled def.			

Table 3. Continued

$[OsO_2F_3][Sb_2F_{11}]$	$[OsO_2F_3][Sb_2F_{11}]$ (C_1)			$Sb_2F_{11}^-$ (C_1)		
exptl[a]	calcd[b] SVWN[f]	calcd[b] B3LYP[g]	assgnts[c,d]	calcd[b] SVWN[f]	calcd[b] B3LYP[h]	assgnts[c,e]
264(7)	243(<1)[42]	276(2)[35]	$\rho_w(F_2OsF_3) + \delta(F_4SbF_9) - \delta(F_{11}Sb'F_{12})$	264(<0.1)[75]	283(<0.1)[77]	$\rho_w(F_5SbF_8) + \rho_w(F_7SbF_9) + \rho_w(F_9Sb'F_{10}) + \rho_w(F_{12}Sb'F_{13})$
255(4)	256(8)[41]	264(1)[26]	$\delta(F_{12}Sb'F_{14}) - \delta(F_{11}Sb'F_{13}) + \rho_t(F_9Sb'F_{10})$	253(2)[8]	271(1)[<0.1]	$\delta(F_6SbF_7) + \delta(F_4SbF_5) + \delta(F_{13}Sb'F_{11}) - \delta(F_{14}Sb'F_{12})$
247 sh, 244(13)	245(12)[26]	264(<1)[31]	$\delta(F_{11}Sb'F_{12}F_{10})$	251(1)[2]	271(1)[<1]	$\delta(F_6SbF_7) + \delta(F_4SbF_5) - \delta(F_{13}Sb'F_{11}) - \delta(F_{14}Sb'F_{12})$
239(4), 238(4)	234(3)[8]	259(1)[13]	$\rho_w(SbF_6F_8F_{13}) + \delta(F_7SbF_7)$	247(1)[10]	266(1)[2]	$\delta_{umb}(SbF_{6,7,8}) + \delta_{umb}(Sb'F_{10,11,12}) - [\delta(F_4SbF_7) + \delta(F_{13}Sb'F_{14})]$
n.o	268(2)[1]	248(1)[132]	$\rho_t(F_5SbF_9) + \delta(F_6SbF_9) + \delta(F_6SbF_8) + \delta_{umb}(Sb'F_{11}F_{12}F_{13}F_{14})$	245(1)[43]	267(1)[<0.1]	$\delta_{umb}(SbF_{4,5,8}) + \delta_{umb}(Sb'F_{10,12,14})$
n.o	226(3)[55]	242(1)[40]		242(<1)[14]	257(<1)[22]	$\delta_{umb}(SbF_{4,5,8}) - \delta_{umb}(Sb'F_{10,12,14})$
n.o.	222(7)[88]	224(1)[76]	$[OsO_2F_3][Sb_2F_{11}]$ coupled def.	233(<1)[12]	254(<0.1)[11]	$[\delta(F_6SbF_8) + \delta(F_4SbF_9)] - [\delta(F_9Sb'F_{14}) + \delta(F_{10}Sb'F_{11})]$
228 (4), 220(8)	199(1)[1]	220(1)[14]		223(<0.1)[192]	243(<0.1)[256]	$\rho_w(F_4SbF_5) + \rho_w(F_6SbF_7) + \rho_w(F_{11}Sb'F_{12}) + \rho_w(F_{13}Sb'F_{14})$
n.o.	190(10)[17]	208(2)[14]	$\delta(F_{10}Sb'F_{11}) - \delta(F_{10}Sb'F_{14})$			
204(5)	178(1)[3]	199(1)[4]		193(1)[<1]	213(1)[<0.1]	
196(5)	187(1)[6]	193(1)[9]	$[OsO_2F_3][Sb_2F_{11}]$ coupled def.	188(1)[1]	212(1)[<0.1]	def. ($Sb_2F_{11}^-$)
190(2)	148(1)[1]	186(<1)[2]		186(1)[2]	183(<1)[<1]	
164(1)	186(9)[11]	167(<1)[8]	$\delta(F_4SbF_7) + \rho_t(F_4SbF_9) + \rho_w(F_5SbF_7)$	157(<1)[<0.1]	174(<0.1)[<0.1]	$[\rho_w(F_8SbF_9) + \rho_w(F_9Sb'F_{10})] - [\rho_w(F_5SbF_7) + \rho_w(F_{12}Sb'F_{13})]$
148(2)	156(1)[<1]	143(1)[<1]	$OsO_2F_3^+$ def.			
137(3)	141(1)[2]	128(<1)[<1]	$\rho_t(F_{11}Sb'F_{13}) - \rho_t(F_{12}Sb'F_{14})$			
n.o	128(1)[1]	125(<1)[2]	$Sb_2F_{11}^-$ coupled def.			
n.o.	119(<1)[3]	121(<0.1)[1]	$[OsO_2F_3][Sb_2F_{11}]$ coupled def.	123(<0.1)[<1]	141(<0.1)[<0.1]	$[\rho_w(F_5SbF_7) + \rho_w(F_{12}Sb'F_{13})] - [\rho_w(F_4SbF_6) + \rho_w(F_{11}Sb'F_{14})]$
n.o.	110(<1)[1]	104(<1)[5]	$Sb_2F_{11}^-$ coupled def./torsion	120(<0.1)[<1]	141(<0.1)[<0.1]	$[\rho_w(F_5SbF_7) + \rho_w(F_{11}Sb'F_{14})] - [\rho_w(F_4SbF_6) + \rho_w(F_{12}Sb'F_{13})]$
n.o.	80(<1)[<1]	98(<1)[1]	$Sb_2F_{11}^-$ coupled def.	110(<1)[<1]	118(1)[<1]	ρ_{rock}(around Sb and Sb')
n.o.	75(<1)[1]	78(<1)[<0.1]	$[OsO_2F_3][Sb_2F_{11}]$ coupled def.			
n.o.	46(1)[1]	60(<1)[1]	$\rho_t(F_1OsF_2) + \rho_r(O_2OsF_3)$	96(<0.1)[<0.1]	104(<0.1)[<0.1]	
n.o.	41(<1)[<0.1]	53(<1)[<0.1]		87(<0.1)[<1]	103(<0.1)[<0.1]	$\rho_{torsion}$(around Sb and Sb')
n.o.	89(<1)[<1]	43(<1)[1]	$[OsO_2F_3][Sb_2F_{11}]$ coupled def.	57(<0.1)[<0.1]	18(<0.1)[<0.1]	
	69(<1)[1]	37(<1)[2]		23(<0.1)[<0.1]	13(<0.1)[<0.1]	
	61(<1)[<1]	32(<1)[<1]	$[OsO_2F_3][Sb_2F_{11}]$ def.			ρ_{rock}(around Sb and Sb')
n.o.	101(1)[<0.1]	30(<0.1)[<1]	$Sb_2F_{11}^-$ coupled def.	34(<0.1)[<0.1]	4(<0.1)[<0.1]	

[a] The Raman spectrum was recorded on a microcrystalline sample in a FEP sample tube at −150 °C using 1064-nm excitation. The experimental Raman intensities (in parentheses) are relative intensities with the most intense band given a value of 100. The abbreviations denote shoulder (sh) and not observed (n.o.). [b] Values in parentheses denote calculated Raman intensities (amu Å^{-4}) and values in square brackets denote calculated infrared intensities (km mol^{-1}). [c] The symbols denote stretch (ν), bend (δ), umbrella (δ_{umb}), and wag (ρ_w). The abbreviation, def., denotes a deformation mode(s). [d] Assignments are based on the B3LYP structure; see Figure 3a for the atom labeling scheme. [e] Assignments are based on the SVWN-optimized structure; see Figure 3c for the atom labeling scheme. [f] SVWN/SDDall(-PP). [g] B3LYP/Stuttgart aug-cc-pVTZ(-PP). [h] B3LYP/aug-cc-pVTZ(-PP).

Ion-pair formation results in pseudo-octahedral coordination about the osmium atom. The bands at 938/941 and 995/997 cm^{-1}, assigned to $\nu(OsO_1) - \nu(OsO_2)$ and $\nu(OsO_1) + \nu(OsO_2)$, respectively, were previously observed at 940 and 996 cm^{-1}, respectively, in a frozen SbF_5 solution.[6] As in the case of *cis*-OsO_2F_4,[17] the in-phase $\nu(OsO_1) + \nu(OsO_2)$ mode is observed at higher frequency than the out-of-phase $\nu(OsO_1) - \nu(OsO_2)$ mode. In contrast with the coupled ν(OsO) modes calculated at the B3LYP level, those calculated at the SVWN level are only weakly coupled and are better described as isolated $\nu(OsO_1)$ and $\nu(OsO_2)$ stretches at this level of theory.

The bands at 702/706/709 and 716/718 cm^{-1}, previously assigned to $Sb_nF_{5n+1}^-$ modes,[6] have been reassigned to the in-phase $\nu(OsF_1) + \nu(OsF_2) + \nu(OsF_3)$ and out-of-phase $\nu(OsF_2) - \nu(OsF_3)$ stretches, respectively. Out-of-phase coupling of the $\nu(OsF_2) + \nu(OsF_3)$ mode to $\nu(OsF_1)$ gives rise to the $\nu(OsF_1) - [\nu(OsF_2) + \nu(OsF_3)]$ mode at 638 cm^{-1}. In general, the Os−O and Os−F stretching modes are in good agreement with those obtained for $OsO_2F_3^+$ in a frozen SbF_5 solution, suggesting that the $OsO_2F_3^+$ cation is fluorine-bridged to the $Sb_nF_{5n+1}^-$ anion and that Os(VIII) is six-coordinate in the latter case.

Frequencies in the ranges 578−608 and 646−696 cm^{-1} are assigned to the Sb−F stretches of $Sb_2F_{11}^-$ and are in good agreement with those reported in the literature.[30,32−35] The prior solution Raman study[6] had assigned a very broad band at 522 cm^{-1} to the out-of-phase stretching mode of the Os---F_b---Sb fluorine bridge, $\nu(OsF_b) - \nu(SbF_b)$. In the present study, this band is resolved into two bands at 500 and 533 cm^{-1}, which have been reassigned. The splitting arises from in-phase and out-of-phase coupling of the out-of-phase component of the Sb---F_9---Sb′ stretching mode of $Sb_2F_{11}^-$, $\nu(Sb'F_9) - \nu(SbF_9)$, with $\nu(OsF_4) - \nu(SbF_4)$. These bridge mode frequencies are similar to the Os---F_b---Os out-of-phase stretching frequencies of [μ-F(*cis*-$OsO_2F_3)_2$][AsF_6] and [μ-F(*cis*-$OsO_2F_3)_2$][Sb_2F_{11}] (492 and 495 cm^{-1}, respectively). In several prior studies of $Sb_2F_{11}^-$ salts, the $\nu(SbF_9) - \nu(Sb'F_9)$ bands were only observed in the infrared spectra of the $Rh(CO_4)^+$ (489 cm^{-1}),[30] $Au(CO)_2^+$ (503 cm^{-1}),[34] and $Pt(CO)_4^+$ (502 cm^{-1})[35] salts, which are in good agreement with the out-of-phase mode assigned in the present study (500 cm^{-1}). The low-frequency deformation modes (137−228 cm^{-1}) consist of coupled cation and anion modes whose frequencies are also in good agreement with the calculated values.

Computational Results. The energy-minimized geometries of [OsO_2F_3][Sb_2F_{11}] (C_1), $Sb_2F_{11}^-$ (C_1), $OsO_2F_3^+$ (C_{2v}) (Figure 3), and [OsO_2F_3][SbF_6] (C_1) (Table S3 and Figure S3) were obtained at the SVWN and B3LYP levels of theory and resulted in stationary points with all frequencies real. The $OsO_2F_3^+$ cation has been previously

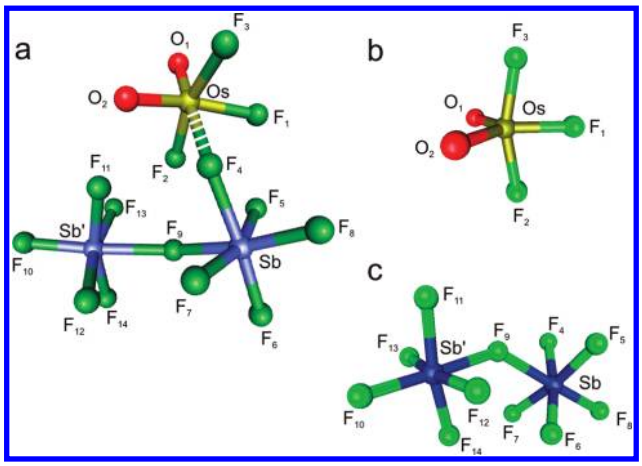

Figure 3. Calculated SVWN/SDDall(-PP) gas-phase geometries for (a) [OsO_2F_3][Sb_2F_{11}] (C_1), (b) $OsO_2F_3^+$ (C_{2v}), and (c) $Sb_2F_{11}^-$ (C_1).

calculated using NLDFT and LDFT methods,[6] and the $Sb_2F_{11}^-$ anion has been calculated at the B3LYP level with the 3-21G* basis set.[29] For consistency and to enable comparisons to be made in the present study, all species have been calculated using more extensive basis sets and at the same levels of theory (see the Experimental Section). All calculated $OsO_2F_3^+$ bond lengths are shorter than those previously calculated and are in better agreement with the experimental values (Table 2). The frequencies calculated at the SVWN level provide slightly better agreement with experimental results than those at the B3LYP level, while the calculated geometries are in equally good agreement with experimental results; therefore, only the SVWN values are referred to in the ensuing discussion.

(a) Calculated Geometries. The gas-phase geometry of $OsO_2F_3^+$ is predicted to be trigonal bipyramidal with two axial fluorine atoms and two oxygen atoms and one fluorine atom in the equatorial plane (Figure 3b). The coordination sphere of osmium in the [OsO_2F_3][Sb_2F_{11}] ion pair is a distorted octahedron that results from a contact to the $Sb_2F_{11}^-$ anion by means of an Os---F_4−Sb bridge (Figure 3a). All of the calculated Os−O and Os−F bond lengths of the ion pair are elongated relative to those of the free cation as a result of electron density donation from the bridge fluorine, F_4, to Os (Table 2). Although the cation of the ion pair and free cation have markedly different calculated geometries, the F_2−Os−F_3 bond angles are bent away from O_1 and O_2 in both cases. The calculated ion-pair structure shows that the atoms in the equatorial plane, [O_2, F_3, F_1, F_2], are displaced away from the axial oxygen (O_1) toward the bridging fluorine atom (F_4) in accordance with the crystal structure.

The calculated Os−O_2 (1.696 Å) and Os−O_1 (1.708 Å) bond lengths are in good agreement with the experimental values (1.654(4) and 1.765(4) Å, respectively). The greater difference observed in the crystal structure is likely the result of short O···F contacts between O(2) and F(7C)/F(10D) of other nearest-neighbor anions in the unit cell.

The Os−F bond lengths of the ion pair are overestimated relative to the experimental values but reproduce the observed trends. Upon ion-pair formation, the Os−F_1

(32) Al-Mukhtar, M.; Holloway, J. H.; Hope, E. G.; Schrobilgen, G. J. *J. Chem. Soc., Dalton Trans.* **1991**, 2831.
(33) Keller, N.; Schrobilgen, G. J. *Inorg. Chem.* **1981**, *20*, 2118–2129.
(34) Willner, H.; Schaebs, J.; Hwang, G.; Mistry, F.; Jones, R.; Trotter, J.; Aubke, F. *J. Am. Chem. Soc.* **1992**, *114*, 8972–8980.
(35) Benkič, P.; Jenkins, H. D. B.; Ponikvar, M.; Mazej, Z. *Eur. J. Inorg. Chem.* **2006**, 1084–1092 and references therein.

bond length is significantly elongated when compared with that of the free cation because the pseudo-octahedral geometry of Os(VIII) places F_1 trans to O_2, whereas for the trigonal bipyramidal gas-phase geometry, F_1, O_1, and O_2 occupy the equatorial plane with $F_1-Os-O_{1,2}$ angles of 125.7°. The $Os-F_2$ (1.835 Å) and $Os-F_3$ (1.852 Å) bond lengths are longer in the gas-phase-ion pair as a result of coordination to and electron donation by the F(4) atom of $Sb_2F_{11}^-$. The $Os-F_{2,3}$ bond lengths are nonequivalent presumably because the F_4---$Os-F_2$ (78.8°) angle is slightly more closed relative to the F_4---$Os-F_3$ (83.7°) angle. The Os---F_4 distance is somewhat underestimated (2.089 Å) when compared with the experimental value (2.190(3) Å). The bond lengths of the Os---F_4-Sb bridge are predicted to be similar, with a calculated $Sb-F_4$ bond length of 2.085 Å for the gas-phase ion pair, 1.958(3) Å for the ion-pair in the experimental structure, and 1.909 Å for the gas-phase $Sb_2F_{11}^-$ anion.

The calculated Sb−F bond lengths of the ion pair are all slightly longer than their experimental values. The asymmetry of the experimental Sb---F_9---Sb′ bridge, Sb---F_9 (1.995(3) Å) and Sb′---F_9 (2.060(3) Å), is reproduced by the calculated Sb---F_9 (2.027 Å) and Sb′---F_9 (2.139 Å) bond lengths. When compared with the bond lengths of the free anion in the gas phase, the Sb−F bond lengths of the ion pair are somewhat shorter because the net anion charge is diminished by bridge formation with the cation. The Sb---F bridge bond lengths of the gas-phase anion are symmetric (2.080 Å) and intermediate with respect to the calculated Sb---F_9---Sb′ bridge bond lengths of the ion pair. The Sb---F_9---Sb′ bond angle of the ion pair is predicted to be significantly more closed (142.0°) than that in the crystal structure (170.0(2)°), which is likely a consequence of close packing in the crystal lattice (vide supra). The bridge angle of the free anion is more closed (133.7°) than that of the ion pair (142.0°) at the SVWN level, while at the B3LYP level, the free anion bond angle is somewhat more open (161.5°) when compared with that of the ion pair (158.2°).

Previous quantum-chemical calculations of the free $Sb_2F_{11}^-$ anion constrained the symmetry to D_{4h} with an Sb---F---Sb angle of 180° and an eclipsed conformation for the two SbF_4 planes.[29] In the current study, the use of C_1 as a starting symmetry allowed the Sb---F---Sb angle to bend and the SbF_4 planes to achieve a staggered conformation. Both structural changes led to better agreement between the observed and calculated bond lengths, angles, and vibrational frequencies. The larger Sb(1)---F(9)---Sb(2) angle in the crystal structure (170.0(2)°) compared to the calculated gas-phase value (133.7)° is likely a consequence of interactions with the cation that accompany cubic close packing, which is indicative of the near-linear Sb(1)---F(9)---Sb(2) angle. The low frequency calculated for the Sb---F---Sb bend (23 cm^{-1}) underscores the deformability of this angle, and its susceptibility to crystal packing.

(b) Charges, Valencies, and Bond Orders. Natural bond orbital (NBO)[36−39] analyses were carried out for the SVWN- and B3LYP-optimized gas-phase structures of $OsO_2F_3^+$, $[OsO_2F_3][Sb_2F_{11}]$, $Sb_2F_{11}^-$ (Table 4), and $[OsO_2F_3][SbF_6]$ (Table S4).

The NBO analyses give natural population analysis (NPA) charges of 2.12 and 1.99 for Os in $OsO_2F_3^+$ and $[OsO_2F_3][Sb_2F_{11}]$, respectively, and 3.08 for Sb in $[OsO_2F_3][Sb_2F_{11}]$ and $Sb_2F_{11}^-$. The average NPA charges of the oxygen ligands are significantly less negative than those of the fluorine ligands in both $OsO_2F_3^+$ and the $[OsO_2F_3][Sb_2F_{11}]$ ion pair, consistent with significant charge transfer from the filled oxygen p orbitals into the empty d orbitals of osmium. The fluorine atom charges of $Sb_2F_{11}^-$ are more negative than those of $OsO_2F_3^+$. The negative charge on F_4 is less than those of the remaining fluorine ligands bonded to Sb because F_4 is bridged to the highly electronegative Os(VIII) center. Overall, the charges are indicative of polar covalent bonds in all three species, with the most polar bonds occurring for the Sb−F and Sb---F bonds.

The average Os−O bond orders (0.89) are approximately double those of the average Os−F (0.50) bond orders, consistent with the formal double-bond characters of the Os−O bonds, which are consistent with the corresponding O and F valencies. The bond orders of Os---F_4 (0.27) and Sb---F_4 (0.26) in the ion pair are similar and indicate a strongly associated ion pair. The anion bridge bonds are asymmetric in the crystal structure, which is reflected in their calculated bond orders, Sb---F_9 (0.39) and Sb′---F_9 (0.22). The higher Sb---F_9 bond order results from electron density withdrawal from Sb by Os through the bridging F_4 atom (vide supra), which strengthens the Sb---F_9 bond and weakens the Sb′---F_9 bond, providing an Sb′−F_9 bond order that is half of the average terminal Sb−F and Sb′−F bond orders (0.45).

(c) Thermochemistries of $[OsO_2F_3][PnF_6]$, $[OsO_2F_3][Sb_2F_{11}]$, $[\mu\text{-}F(OsO_2F_3)_2][PnF_6]$, and $[\mu\text{-}F(OsO_2F_3)_2][Sb_2F_{11}]$ (Pn = As, Sb). Attempts to synthesize $[OsO_2F_3][SbF_6]$ from *cis*-OsO_2F_4 and SbF_5 under various conditions have proven unsuccessful (see Synthesis of $[OsO_2F_3][Sb_2F_{11}]$ and Attempted Synthesis of $[OsO_2F_3][SbF_6]$), resulting in the formation of either $[OsO_2F_3][Sb_2F_{11}]$ or $[\mu\text{-}F(OsO_2F_3)_2][Sb_2F_{11}]$. To account for the preferential formation of $Sb_2F_{11}^-$ salts, quantum-chemical calculations and volume-based lattice energies[40,41] were used in conjunction with known thermodynamic quantities to estimate the standard enthalpies listed in Scheme 1.

The standard enthalpies were estimated by analyzing the corresponding Born−Haber cycles as exemplified for $\Delta H°_2$ in Scheme 2. The enthalpies of fluoride ion abstraction from *cis*-OsO_2F_4 ($\Delta H°_{-F^-}$), fluoride ion attachment ($\Delta H°_{+F^-}$) to the Lewis acids MF_5 (M = Sb or As), association of the SbF_6^- ion with SbF_5 ($\Delta H°_{+Sb_2F_{11}^-}$), and association of the $OsO_2F_3^+$ cation with *cis*-OsO_2F_4 ($\Delta H°_{+Os_2O_4F_7^+}$) were calculated at the SVWN and B3LYP

(36) Glendening, E. D.; Reed, A. E.; Carpenter, J. E.; Weinhold, F. In *NBO*, version 3.1; Gaussian Inc.: Pittsburgh, PA, 1990.
(37) Reed, A. E.; Curtiss, L. A.; Weinhold, F. *Chem. Rev.* **1998**, *88*, 899–926.
(38) Reed, A. E.; Weinstock, R. B.; Weinhold, F. *J. Chem. Phys.* **1985**, *83*, 735–746.
(39) Glendening, E. D.; Badenhoop, J. K.; Reed, A. E.; Carpenter, J. E.; Bohmann, C. M.; Morales, C. M.; Weinhold, F. In *NBO*, version 5.0; Theoretical Chemical Institute, University of Wisconsin: Madison, WI, 2001.
(40) Jenkins, H. D. B. *Inorg. Chem.* **1999**, *38*, 3609–3620.
(41) Jenkins, H. D. B.; Tudela, D.; Glasser, L. *Inorg. Chem.* **2002**, *41*, 2364–2367.

Table 4. Natural Bond Orbital (NBO) Valencies, Bond Orders, and NPA Charges for $OsO_2F_3^+$, $[OsO_2F_3][Sb_2F_{11}]$, and $Sb_2F_{11}^-$

Charges						
	$OsO_2F_3^+$ (C_{2v})		$[OsO_2F_3][Sb_2F_{11}]$ (C_1)		$Sb_2F_{11}^-$ (C_1)	
atom	SVWN	B3LYP	SVWN	B3LYP	SVWN	B3LYP
Os	2.12	2.43	1.99	2.31		
O_1	−0.16	−0.21	−0.21	−0.23		
O_2	−0.16	−0.21	−0.18	−0.20		
F_1	−0.29	−0.36	−0.34	−0.41		
F_2	−0.25	−0.33	−0.29	−0.34		
F_3	−0.25	−0.33	−0.32	−0.38		
F_4			−0.58	−0.62	−0.64	−0.64
Sb			3.08	3.07	3.08	3.06
F_5			−0.61	−0.61	−0.64	−0.64
F_6			−0.61	−0.61	−0.65	−0.64
F_7			−0.60	−0.60	−0.65	−0.64
F_8			−0.62	−0.62	−0.66	−0.66
F_9			−0.67	−0.66	−0.66	−0.67
Sb′			3.08	3.05	3.08	3.06
F_{10}			−0.63	−0.63	−0.66	−0.66
F_{11}			−0.62	−0.62	−0.65	−0.64
F_{12}			−0.62	−0.62	−0.64	−0.64
F_{13}			−0.63	−0.65	−0.65	−0.64
F_{14}			−0.62	−0.63	−0.64	−0.64
Valencies						
	$OsO_2F_3^+$ (C_{2v})		$[OsO_2F_3][Sb_2F_{11}]$ (C_1)		$Sb_2F_{11}^-$ (C_1)	
atom	SVWN	B3LYP	SVWN	B3LYP	SVWN	B3LYP
Os	3.33	3.26	3.52	3.55		
O_1	0.95	0.96	0.95	0.96		
O_2	0.95	0.96	0.96	0.94		
F_1	0.54	0.52	0.50	0.47		
F_2	0.55	0.50	0.56	0.52		
F_3	0.55	0.50	0.53	0.50		
F_4			0.51	0.49	0.38	0.32
Sb			2.40	2.61	2.49	2.14
F_5			0.38	0.43	0.38	0.32
F_6			0.40	0.45	0.38	0.32
F_7			0.39	0.44	0.38	0.32
F_8			0.39	0.44	0.38	0.33
F_9			0.43	0.52	0.46	0.41
Sb′			2.45	2.62	2.49	2.14
F_{10}			0.40	0.44	0.38	0.33
F_{11}			0.39	0.42	0.38	0.32
F_{12}			0.40	0.42	0.38	0.32
F_{13}			0.37	0.38	0.38	0.32
F_{14}			0.38	0.41	0.38	0.32
Bond Orders						
	$OsO_2F_3^+$ (C_{2v})		$[OsO_2F_3][Sb_2F_{11}]$ (C_1)		$Sb_2F_{11}^-$ (C_1)	
bond	SVWN	B3LYP	SVWN	B3LYP	SVWN	B3LYP
Os−O_1	0.89	0.89	0.90	0.92		
Os−O_2	0.89	0.89	0.88	0.91		
Os−F_1	0.51	0.48	0.48	0.46		
Os−F_2	0.52	0.49	0.52	0.51		
Os−F_3	0.52	0.49	0.50	0.49		
Os---F_4			0.27	0.27		
Sb−F_4			0.26	0.26	0.44	0.38
Sb−F_5			0.44	0.49	0.44	0.38
Sb−F_6			0.45	0.50	0.44	0.38
Sb−F_7			0.45	0.50	0.44	0.38
Sb−F_8			0.44	0.49	0.43	0.38
Sb---F_9			0.39	0.37	0.27	0.24
Sb′---F_9			0.22	0.22	0.27	0.24
Sb′−F_{10}			0.45	0.49	0.43	0.38
Sb′−F_{11}			0.46	0.49	0.44	0.38
Sb′−F_{12}			0.46	0.49	0.44	0.38
Sb′−F_{13}			0.39	0.46	0.44	0.38
Sb′−F_{14}			0.44	0.48	0.44	0.38

Scheme 1. Summary of Reactions for Which Standard Enthalpies Have Been Calculated

ΔH°_1	$OsO_2F_{4(s)} + SbF_{5(l)}$	⟶	$[OsO_2F_3][SbF_6]_{(s)}$
ΔH°_2	$OsO_2F_{4(s)} + 2SbF_{5(l)}$	⟶	$[OsO_2F_3][Sb_2F_{11}]_{(s)}$
ΔH°_3	$2OsO_2F_{4(s)} + SbF_{5(l)}$	⟶	$[\mu\text{-}(OsO_2F_3)_2][SbF_6]_{(s)}$
ΔH°_4	$2OsO_2F_{4(s)} + 2SbF_{5(l)}$	⟶	$[\mu\text{-}(OsO_2F_3)_2][Sb_2F_{11}]_{(s)}$
ΔH°_5	$OsO_2F_{4(s)} + AsF_{5(g)}$	⟶	$[OsO_2F_3][AsF_6]_{(s)}$
ΔH°_6	$2OsO_2F_{4(s)} + AsF_{5(g)}$	⟶	$[\mu\text{-}(OsO_2F_3)_2][AsF_6]_{(s)}$
ΔH°_7	$2[OsO_2F_3][SbF_6]_{(s)}$	⟶	$[\mu\text{-}(OsO_2F_3)_2][Sb_2F_{11}]_{(s)}$

Scheme 2. Thermochemical Cycle Describing the Formation of $[OsO_2F_3][Sb_2F_{11}]$

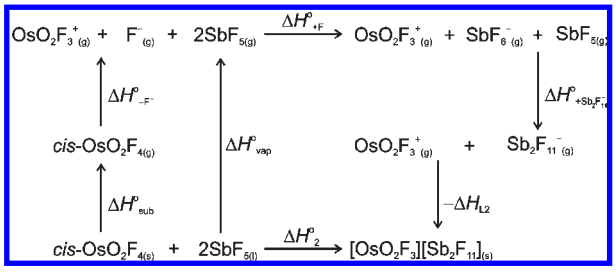

Table 5. Gas-Phase Reaction Enthalpies for Fluoride Ion Transfer Reactions Involving *cis*-OsO_2F_4, SbF_5, and AsF_5

ΔH° (kJ mol^{-1})		
	SVWN[a]	B3LYP[b]
$OsO_2F_{4(g)} \rightarrow OsO_2F_3^+{}_{(g)} + F^-{}_{(g)}$	699	918
$OsO_2F_{4(g)} + OsO_2F_3^+{}_{(g)} \rightarrow \mu\text{-}F(OsO_2F_3)_2^+{}_{(g)}$	−182	−113
$SbF_{5(g)} + F^-{}_{(g)} \rightarrow SbF_6^-{}_{(g)}$	−571	−464
$SbF_{5(g)} + SbF_6^-{}_{(g)} \rightarrow Sb_2F_{11}^-{}_{(g)}$	−522	−132
$AsF_{5(g)} + F^-{}_{(g)} \rightarrow AsF_6^-{}_{(g)}$	−190	−406

[a] Zero-point energy-corrected enthalpies calculated using the SDDall basis set augmented for F, O, and Sb with two d-type polarization functions. [b] Zero-point energy-corrected enthalpies calculated using the Stuttgart basis set with the f functional for Os and the aug-cc-pVTZ(-PP) basis sets for all other atoms.

(Table 5) levels of theory. The SVWN and B3LYP values differ but follow the same trends, with the B3LYP values expected to give more reliable energies.[42] Consequently, only the B3LYP values are referred to in the ensuing discussion.

The lattice enthalpies of the $OsO_2F_3^+$ and μ-$F(OsO_2F_3)_2^+$ salts (Table 6) were estimated by use of the volume-based method of Bartlett et al.[43] as generalized by Jenkins et al.[40,41] in eq 6, where R is the gas constant (8.314 J K^{-1} mol^{-1}); V_m is the volume of the salt; I is the ionicity of the salt (1); and α (117.3 mm kJ mol^{-1}), β (51.9 kJ mol^{-1}), and p (2) depend on the nature of the salt. In this formalism, ΔH_L, the lattice enthalpy, is defined as the energy required to break apart the crystal lattice and therefore has a positive value. The determination of the enthalpy of vaporization of SbF_5 (ΔH°_{vap}) is complicated by the polymeric nature of liquid SbF_5 and has been

(42) Riedel, S.; Kaupp, M. *Inorg. Chem.* **2006**, *45*, 10497–10502.
(43) Bartlett, N.; Yeh, S.; Kourtakis, K.; Mallouk, T. *J. Fluorine Chem.* **1984**, *26*, 97–116.

Table 6. Estimated Volumes and Lattice Enthalpies of Salts Containing the $OsO_2F_3^+$ and μ-$F(OsO_2F_3)_2^+$ Cations

	salt	V_m (nm^3)[a]	ΔH_L (kJ mol^{-1})[b]
ΔH_{L1}	$[OsO_2F_3][SbF_6]$	0.1627	538.5
ΔH_{L2}	$[OsO_2F_3][Sb_2F_{11}]$	0.26870(2)	472.3
ΔH_{L3}	$[\mu\text{-}F(OsO_2F_3)_2][SbF_6]$	0.2817	466.6
ΔH_{L4}	$[\mu\text{-}F(OsO_2F_3)_2][Sb_2F_{11}]$	0.3877(2)	430.5
ΔH_{L5}	$[OsO_2F_3][AsF_6]$	0.1517	548.6
ΔH_{L6}	$[\mu\text{-}F(OsO_2F_3)_2][AsF_6]$	0.2707	471.4

[a] The formula unit volumes, V_m, for $[OsO_2F_3][Sb_2F_{11}]$ (0.26870(2) nm^3) and $[\mu\text{-}F(OsO_2F_3)_2][Sb_2F_{11}]$ (0.3877(2) nm^3)[6] were obtained from their crystallographic unit cells at −173 °C. The volumes of SbF_6^- (0.121(12) nm^3) and AsF_6^- (0.110(7) nm^3) were obtained from ref 40, and the volume of $Sb_2F_{11}^-$ (0.227 nm^3) was obtained from ref 44. The volumes of $OsO_2F_3^+$ (0.0417 nm^3) and μ-$(OsO_2F_3)_2^+$ (0.1607 nm^3) were estimated by subtraction of the SbF_6^- and $Sb_2F_{11}^-$ anion volumes, respectively, from V_m. The V_m values for the $[OsO_2F_3][SbF_6]$, $[\mu\text{-}F(OsO_2F_3)_2][SbF_6]$, $[OsO_2F_3][AsF_6]$, and $[\mu\text{-}F(OsO_2F_3)_2][AsF_6]$ salts were estimated from the sums of the respective cation and anion volumes. [b] The lattice enthalpies (ΔH_L) were calculated from eq 8 as described in ref 41.

Table 7. Reaction Enthalpies for the Formation of the AsF_6^-, SbF_6^-, and $Sb_2F_{11}^-$ Salts of $OsO_2F_3^+$ and μ-$F(OsO_2F_3)_2^+$

reaction enthalpies[a]	SVWN[b]	B3LYP[b]
$\Delta H°_1$	$\Delta H_{sub} - 379$	$\Delta H_{sub} - 54.0$
$\Delta H°_2$	$\Delta H_{sub} - 804$	$\Delta H_{sub} - 89.0$
$\Delta H°_3$	$2\Delta H_{sub} - 490$	$2\Delta H_{sub} - 95.0$
$\Delta H°_4$	$2\Delta H_{sub} - 944$	$2\Delta H_{sub} - 160$
$\Delta H°_5$	$\Delta H_{sub} - 39.0$	$\Delta H_{sub} - 37.3$
$\Delta H°_6$	$2\Delta H_{sub} - 144$	$2\Delta H_{sub} - 73.0$
$\Delta H°_7$	−185	−52.1

[a] See Scheme 1 for the reaction details. [b] Values are in kJ mol^{-1}.

previously estimated to be 30.9 kJ mol^{-1}.[44−48] The determination of the enthalpy of sublimation of *cis*-OsO_2F_4 ($\Delta H°_{sub}$) is prevented because *cis*-OsO_2F_4 decomposes near its melting point (90 °C).[17] Consequently, enthalpies of reaction, $\Delta H°$, have been calculated incorporating values for all components of their Born−Haber cycles except $\Delta H°_{sub}$ of *cis*-OsO_2F_4 (Table 7).

$$\Delta H_L = 2I\left(\frac{\alpha}{\sqrt[3]{V_m}} + \beta\right) + pRT \qquad (6)$$

The enthalpies of reaction for the formation of $OsO_2F_3^+$ and μ-$F(OsO_2F_3)_2^+$ salts can be calculated using thermochemical cycles similar to that given in Scheme 2 and are summarized by eq 7. Because the $\Delta H°_{sub}$ of *cis*-OsO_2F_4 is unknown, direct comparisons of the reaction enthalpies for a pair of reactions involving different molar amounts of *cis*-OsO_2F_4 in their reactions are not possible. For a pair of reactions having equimolar amounts of *cis*-OsO_2F_4 in common as a reactant, taking the difference in their reaction enthalpies leads to cancellation of the $\Delta H°_{sub}$ term and to the difference in their reaction enthalpies (Table 8).

Table 8. Comparisons of $\Delta H°$ Values for Reactions that Lead to $OsO_2F_3^+$ and μ-$F(OsO_2F_3)_2^+$ Salt Formation

	$\Delta(\Delta H°)$	
standard enthalpy difference[a]	SVWN[b]	B3LYP[b]
$\Delta H°_2 - \Delta H°_1$	−424	−35.0
$\Delta H°_1 - \Delta H°_5$	−340	−16.7
$\Delta H°_2 - \Delta H°_5$	−765	−51.7
$\Delta H°_4 - \Delta H°_3$	−454	−65.1
$\Delta H°_3 - \Delta H°_6$	−346	−22.0
$\Delta H°_4 - \Delta H°_6$	−800	−87.1

[a] See Scheme 1 for the reaction details. [b] Values are in kJ mol^{-1}.

Scheme 3. Thermochemical Cycle Describing the Conversion of $[OsO_2F_3][SbF_6]$ to $[\mu\text{-}F(OsO_2F_3)_2][Sb_2F_{11}]$

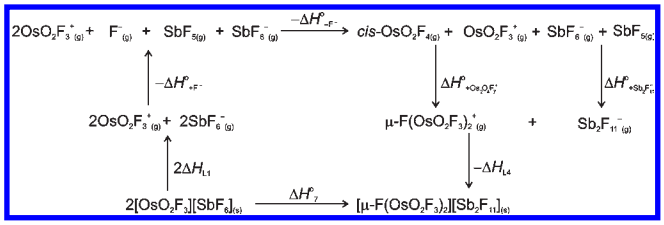

$$\Delta H°_2 = 2\Delta H°_{vap} + \Delta H°_{sub} + \Delta H°_{-F^-} + \Delta H°_{+F^-} + \Delta H°_{+SbF_6^-} - \Delta H_{L2} \qquad (7)$$

Examination of Table 8 reveals that the formation of $[OsO_2F_3][Sb_2F_{11}]$ and $[\mu\text{-}F(OsO_2F_3)_2][Sb_2F_{11}]$ is favored relative to that of $[OsO_2F_3][SbF_6]$ (−35.0 kJ mol^{-1}) and $[\mu\text{-}F(OsO_2F_3)_2][SbF_6]$ (−65.1 kJ mol^{-1}), in accordance with one's ability to isolate stable $[OsO_2F_3][Sb_2F_{11}]$ and $[\mu\text{-}F(OsO_2F_3)_2][Sb_2F_{11}]$[6] salts and inability to form the $[OsO_2F_3][SbF_6]$ and $[\mu\text{-}F(OsO_2F_3)_2][SbF_6]$ salts.

The standard enthalpies of reaction leading to the formation of the AsF_6^- salts of $OsO_2F_3^+$ and μ-$F(OsO_2F_3)_2^+$ ($\Delta H°_5$ and $\Delta H°_6$, respectively) are less favorable when compared with their SbF_6^- and $Sb_2F_{11}^-$ analogs (Table 8). Direct comparisons of the standard enthalpies for the reactions of *cis*-OsO_2F_4 and AsF_5 that lead to the AsF_6^- salts of $OsO_2F_3^+$ and μ-$F(OsO_2F_3)_2^+$, however, are also not possible because the $\Delta H°_{sub}$ of *cis*-OsO_2F_4 is unknown. Although $[OsO_2F_3][AsF_6]$ is presently unknown, $[\mu\text{-}F(OsO_2F_3)_2][AsF_6]$ has been isolated and characterized by low-temperature Raman spectroscopy.[6] This salt has a significant AsF_5 dissociation vapor pressure (150 Torr, 23 °C) in accordance with its less negative enthalpy of reaction relative to those of the SbF_6^- and $Sb_2F_{11}^-$ analogues (Table 8).

Because an explicit comparison of the enthalpies of reaction for the formation of $[OsO_2F_3][SbF_6]$ and $[\mu\text{-}F(OsO_2F_3)_2][Sb_2F_{11}]$ is not possible, an alternative thermochemical cycle was considered (Scheme 3) that allowed the enthalpy for the interconversion of $[OsO_2F_3][SbF_6]$ and $[\mu\text{-}F(OsO_2F_3)_2][Sb_2F_{11}]$, $\Delta H°_7$ (eq 8), to be estimated. The $\Delta H°_7$ value (−52.1 kJ mol^{-1}) indicates that the formation of $[\mu\text{-}F(OsO_2F_3)_2][Sb_2F_{11}]$ from $[OsO_2F_3][SbF_6]$ is also an exothermic process, again

(44) Lehmann, J. F.; Riedel, S.; Schrobilgen, G. J. *Inorg. Chem.* **2008**, *47*, 8343–8356.
(45) Shair, R. C.; Schurig, W. F. *Ind. Eng. Chem.* **1951**, *43*, 1624–1627.
(46) Brunvoll, J.; Ischenko, A. A.; Miakshin, I. N.; Romanov, G. V.; Spiridonov, V. P.; Strand, T. G.; Sukhoverkhov, V. F. *Acta Chem. Scand. A* **1980**, *34*, 733–737.
(47) Fawcett, J.; Holloway, J. H.; Peacock, R. D.; Russell, D. K. *J. Fluorine Chem.* **1982**, *20*, 9–12.
(48) Bougon, R.; Bui Huy, T.; Burgess, J.; Christe, K. O.; Peacock, R. D. *J. Fluorine Chem.* **1982**, *19*, 263–277.

underscoring why all attempts to synthesize $[OsO_2F_3][SbF_6]$ have led to $[\mu\text{-}F(OsO_2F_3)_2][Sb_2F_{11}]$ as the only isolable product.

$$\Delta H^\circ_7 = 2\Delta H_{L1} + \Delta H^\circ_{+OsO_2F_3^+} + \Delta H^\circ_{+SbF_6^-} - (\Delta H^\circ_{-F^-} + \Delta H^\circ_{+F^-} + \Delta H_{L4}) \quad (8)$$

A method for estimating the absolute standard entropy of a salt from its formula unit volume has been reported by Jenkins and Glasser (eq 9), where k is 1360 J K^{-1} mol^{-1} nm^{-3} and c is 15 J K^{-1} mol^{-1}.[49]

$$S^\circ([Os_nO_{2n}F_{4n-1}][Sb_nF_{5n+1}]) = kV_m + c \quad (9)$$

The entropies calculated by this method for $[OsO_2F_3][SbF_6]$ and $[\mu\text{-}F(OsO_2F_3)_2][Sb_2F_{11}]$ are 236 and 542 JK^{-1} mol^{-1}, respectively. The estimated ΔS° for the conversion of $[OsO_2F_3][SbF_6]$ to $[\mu\text{-}F(OsO_3F_2)_2][Sb_2F_{11}]$ (eq 11) is 69.7 J K^{-1} mol^{-1}, leading to a ΔG° value (eq 10) of -206 kJ mol^{-1} at the SVWN level and -72.8 kJ mol^{-1} at the B3LYP level. Gibbs free energies for the remaining reaction pairs in Table 8 cannot be evaluated because $S^\circ(SbF_{5(l)})$ is unknown. The only values available are those for the gas-phase monomer (353 J K^{-1} mol^{-1})[50] and the gas-phase tetramer (-35.5 J K^{-1} mol^{-1}).[47]

$$\Delta G^\circ = \Delta H^\circ - T\Delta S^\circ \quad (10)$$

$$2[OsO_2F_3][SbF_6]_{(s)} \longrightarrow [\mu\text{-}(OsO_2F_3)_2][Sb_2F_{11}]_{(s)} \quad (11)$$

Conclusions

The $OsO_2F_3^+$ cation, previously observed in SbF_5 solution by ^{19}F NMR spectroscopy, has been fully structurally characterized in the solid state as its $Sb_2F_{11}^-$ salt. The $[OsO_2F_3][Sb_2F_{11}]$ structural unit is an ion pair in which a *cis*-dioxo $OsO_2F_3^+$ cation is fluorine-bridged to an $Sb_2F_{11}^-$ anion, resulting in a pseudo-octahedral coordination sphere for Os(VIII). The Raman spectrum of the $Sb_2F_{11}^-$ salt has been fully assigned on the basis of the calculated vibrational frequencies of the gas-phase $[OsO_2F_3][Sb_2F_{11}]$ ion pair. The gas-phase geometry and vibrational frequencies of $Sb_2F_{11}^-$ are in good agreement with the anion in $[OsO_2F_3][Sb_2F_{11}]$. The calculated vibrational frequencies of $Sb_2F_{11}^-$ are in better agreement with experiment than those previously reported, and provide more reliable vibrational assignments. Attempts to prepare $[OsO_2F_3][SbF_6]$ were unsuccessful and only resulted in the isolation of $[\mu\text{-}F(OsO_2F_3)_2][Sb_2F_{11}]$. Thermochemical calculations demonstrate that the standard enthalpies of reaction that lead to the $Sb_2F_{11}^-$ salts of $OsO_2F_3^+$ and $\mu\text{-}F(OsO_2F_3)_2^+$ are favored over the AsF_6^- and SbF_6^- salts, in accordance with failures to form $[OsO_2F_3][SbF_6]$ and $[\mu\text{-}F(OsO_2F_3)_2][SbF_6]$ in the present study.

Experimental Section

Apparatus and Materials. Manipulations involving air-sensitive materials were carried out under anhydrous conditions as previously described.[6] All preparative work was carried out in FEP fluoroplastic vessels fabricated from ¼-in. o.d. lengths of FEP tubing which had been fashioned into either cylindrical reaction tubes or "beaded" sample tubes for crystal growth. Both types of reaction vessel were heat-sealed at one end and connected through 45° SAE flares to Kel-F valves. A typical "beaded" vessel was fashioned from a ¼-in. o.d. FEP reaction tube by blowing three consecutive 8 to 9-mm-diameter bubbles, having center-to-center distances of 10 to 20 mm, into heated portions of the tube commencing near the heat-sealed end of the vessel (see Crystal Growth). Reaction vessels were dried on a Pyrex glass vacuum line and were then transferred to a metal vacuum line where they were passivated with F_2 for several hours, refilled with dry N_2, and placed in a drybox until used. Vessels were connected to a vacuum line by means of ¼-in. 316 stainless steel Swagelok Ultratorr unions fitted with Viton O-rings.

Antimony pentafluoride (Ozark-Mahoning Co.) was purified by vacuum distillation as previously described,[51] and *cis*-OsO_2F_4 was synthesized by the reaction of OsO_4 (Koch-Light, 99.6%) with KrF_2 in aHF, as previously described.[17] Anhydrous HF (Harshaw Chemicals Co.) was purified as previously described.[52]

Synthesis of $[OsO_2F_3][Sb_2F_{11}]$. A fluorine-passivated ¼-in. o.d. FEP reaction tube was loaded with 0.1055 g (0.3541 mmol) of deep burgundy colored *cis*-OsO_2F_4 inside a nitrogen-filled drybox. The reaction tube was then transferred to a glovebag purged with dry N_2, and an excess of SbF_5, 0.500 g (2.31 mmol), was syringed into the tube. Upon warming the reactor and contents to room temperature, *cis*-OsO_2F_4 slowly dissolved, giving a deep orange solution having a significantly lower viscosity than that of pure SbF_5, which was indicative of $Sb_nF_{5n+1}^-$ anion formation. The reaction vessel was pumped at 0 °C to remove excess SbF_5. After pumping for 40 h, 0.2559 g (0.3498 mmol) of orange powder remained, which was identified as $[OsO_2F_3][Sb_2F_{11}]$ (98.8% yield) by Raman spectroscopy.

Attempted Syntheses of $[OsO_2F_3][SbF_6]$. Following a procedure similar to that outlined above, 0.0602 g (0.202 mmol) of *cis*-OsO_2F_4 was loaded into a reaction tube followed by the addition of 0.5056 g (2.333 mmol) of SbF_5. After warming the reactor and contents to room temperature, *cis*-OsO_2F_4 slowly dissolved in SbF_5, giving a deep orange solution, which had a significantly lower viscosity than pure SbF_5. Excess SbF_5 was removed by pumping at 0 °C for 3 days, yielding an orange powder identified by Raman spectroscopy as $[OsO_2F_3][Sb_2F_{11}]$. Further pumping on the sample followed by periodic weighing and characterization by Raman spectroscopy revealed a loss of SbF_5 from the sample. After 6 days of pumping, an orange powder (0.1110 g) remained, which was identified by Raman spectroscopy as $[\mu\text{-}F(OsO_2F_3)_2][Sb_2F_{11}]$ (0.1078 mmol; 107% yield).

In another attempt to isolate $[OsO_2F_3][SbF_6]$, 0.06635 g (0.2251 mmol) of *cis*-OsO_2F_4 was transferred into a ¼-in. o.d. FEP reaction vessel equipped with an FEP side arm fused to the main tube, and excess SbF_5 (ca. 0.25 g, 1.16 mmol) was added, followed by the condensation of ca. 1 mL of aHF onto the sample at -196 °C. Upon warming to room temperature, the sample rapidly dissolved to give a light orange solution. The sample was cooled to -78 °C, whereupon a light orange solid precipitated. The Raman spectrum of the solid was recorded under aHF at -150 °C and was shown to be $[\mu\text{-}F(OsO_2F_3)_2][Sb_2F_{11}]$. Excess HF and SbF_5 were removed under dynamic vacuum at 0 °C. Pumping for 5 h yielded a free-flowing orange powder (0.1152 g) identified by Raman spectroscopy as $[\mu\text{-}F(OsO_2F_3)_2][Sb_2F_{11}]$ (0.1119 mmol; 99.4% yield).

(49) Jenkins, H. D. B.; Glasser, L. *Inorg. Chem.* **2003**, *42*, 8702–8708.
(50) Nagarajan, G. *Bull. Soc. Chim. Belg.* **1962**, *71*, 324–328.
(51) Gillespie, R. J.; Netzer, A.; Schrobilgen, G. J. *Inorg. Chem.* **1974**, *13*, 1455–1459.
(52) Emara, A. A. A.; Schrobilgen, G. J. *Inorg. Chem.* **1992**, *31*, 1323–1332.

In a final attempt to synthesize $[OsO_2F_3][SbF_6]$, $[OsO_2F_3][Sb_2F_{11}]$ was prepared from 0.06404 g (0.2148 mmol) of *cis*-OsO_2F_4 and an excess of SbF_5 (ca. 0.25 g, 1.16 mmol) in a ¼-in. o.d. FEP reaction tube, as previously described (vide supra). Two equivalents of *cis*-OsO_2F_4 (0.1201 g, 0.4027 mmol) were added to freshly prepared $[OsO_2F_3][Sb_2F_{11}]$ (0.1520 g, 0.2077 mmol) followed by the condensation of ca. 1 mL of aHF onto the sample at −196 °C. Upon warming to room temperature, the sample slowly dissolved to give a purple-colored solution. The sample was cooled to −78 °C, whereupon a purple solid corresponding to *cis*-OsO_2F_4 precipitated. The Raman spectrum was recorded under aHF at −150 °C and showed that a mixture of $[\mu\text{-}F(OsO_2F_3)_2][Sb_2F_{11}]$ and *cis*-OsO_2F_4 was present. Hydrogen fluoride removal under dynamic vacuum at −78 °C followed by pumping for 3 h at −78 °C yielded a finely divided mixture of orange and purple crystallites identified by Raman spectroscopy as $[\mu\text{-}F(OsO_2F_3)_2][Sb_2F_{11}]$[6] and *cis*-$OsO_2F_4$.[15] Upon warming to 90 °C for 1 h, the sample turned completely purple as *cis*-OsO_2F_4 neared its melting point. The Raman spectrum (−150 °C) of the heated mixture showed no signs that further reaction had occurred.

Raman Spectroscopy. Low-temperature Raman spectra were recorded at −150 °C on a Bruker RFS 100 FT Raman spectrometer using 1064-nm excitation and a resolution of 1 cm^{-1}, as previously described.[53] The spectra were recorded using a laser power of 300 mW and a total of 1200 scans.

X-ray Crystal Structure Determination of $[OsO_2F_3][Sb_2F_{11}]$. **(a) Crystal Growth.** Crystals of $[OsO_2F_3][Sb_2F_{11}]$ were obtained from a sample composed of 0.0821 g (0.275 mmol) of *cis*-OsO_2F_4 and excess SbF_5 (0.500 g, 2.31 mmol) in a ¼-in. o.d. FEP beaded reactor (vide supra). The sample was placed in a near-horizontal position, distributing the SbF_5 solution equally among the three wells of the beaded reactor. Slow removal of SbF_5 under dynamic vacuum at 0 °C resulted in crystal growth within each well. After 30 h, SbF_5 solvent had been completely removed and pumping was halted. The tube and orange crystalline samples were cooled to −78 °C and back-filled with dry N_2.

(b) Collection and Reduction of X-ray Data. A crystal of $[OsO_2F_3][Sb_2F_{11}]$ having the dimensions 0.26 × 0.12 × 0.06 mm^3 was selected at −105 ±3 °C for low-temperature X-ray structure determination and was mounted in a cold stream (−173 °C) on a goniometer head as previously described.[53] The crystal was centered on a P4 Siemens diffractometer, equipped with a Siemens SMART 1K CCD area detector, controlled by SMART,[54] and a rotating anode emitting Kα radiation monochromated (λ = 0.71073 Å) by a graphite crystal. Diffraction data collection (at −173 °C) consisted of a full ψ rotation at $\chi = 0°$ using (1040 + 30) 0.3° frames, followed by a series of short (80 frames) ω scans at various ψ and χ settings to fill the gaps. The crystal-to-detector distance was 5.012 cm, and the data collection was carried out in a 512 × 512 pixel mode using 2 × 2 pixel binning. Raw data were processed using SAINT+,[54] which applied Lorentz and polarization corrections to three-dimensionally integrated diffraction spots. The program SADABS[55] was used for the scaling of diffraction data, the application of a decay correction, and an empirical absorption correction based on the intensity ratios of redundant reflections.

(c) Solution and Refinement of the Structure. The XPREP program was used to confirm the unit cell dimensions and the crystal lattice. The solution was obtained by direct methods which located the positions of the atoms defining the $OsO_2F_3^+$ cation and the $Sb_2F_{11}^-$ anion. The final refinement was obtained by introducing anisotropic thermal parameters and the recommended weightings for all of the atoms. The maximum electron densities in the final difference Fourier map were located near the heavy atoms. All calculations were performed using the SHELXTL-plus package[56] for the structure determination and solution refinement and for the molecular graphics. The choice of space group was further confirmed using PLATON as implemented within the WinGX software package.[57]

X-ray Powder Diffraction. **(a) Sample Preparation.** A microcrystalline sample of $[OsO_2F_3][Sb_2F_{11}]$ was freshly prepared by dissolution of 0.1056 g (0.3540 mmol) of *cis*-OsO_2F_4 in 0.503 g (2.32 mmol) of SbF_5 followed by removal of excess SbF_5, as previously described. A low-temperature mounting technique similar to that described for mounting thermally unstable or moisture-sensitive single crystals[53] was used to mount a powdered sample. The cold (−78 °C) sample tube was cut open under a dry argon stream and dumped onto an aluminum trough cooled by a dry nitrogen cold stream (−105 ±3 °C). The closed end of a 0.3 mm glass capillary was attached by means of epoxy to a metallic pin having a magnetic interface. The flat edge of a stainless steel stylus was used to crush the microcrystalline sample, and the powdered material was forced into the open end of the mounted capillary to a depth of ca. 2 mm under the nitrogen cold stream. The sample was quickly transferred to the goniometer head of the X-ray diffractometer by means of a cryotongs, previously cooled to −196 °C, and attached to the magnetic interface of the goniometer head.

(b) Collection and Processing of X-ray Powder Data. The powdered sample (vide supra) was centered on a Bruker SMART APEX II diffractometer, equipped with an APEX II 4K CCD area detector and a triple-axis goniometer, controlled by the APEX2 Graphical User Interface (GUI) software,[58] and a sealed source emitting graphite-monochromated Mo Kα radiation (λ = 0.71073 Å). Diffraction data were collected at −150 °C and consisted of a 360° rotation for φ and fixed χ, 2θ, and ω angles of 54.76°, 18°, and 9°, respectively. The sample was also equilibrated at −173 °C for 30 min, and the data collection was repeated. The sample-to-detector distance was 16.940 cm, and the data collection was carried out in a 512 × 512 pixel mode using 2 × 2 pixel binning. The two-dimensional powder analysis and integration around χ was completed using the GADDS[59] program, resulting in a standard one-dimensional intensity versus 2θ plot. The powder pattern was calculated for the single-crystal data using the Mercury[60] program and was compared with the powder data using the TOPAS[61] program (Figure S2).

Computational Methods. The optimized geometries, frequencies, and zero-point energy-corrected enthalpies of F^-, *cis*-OsO_2F_4, $OsO_2F_3^+$, $\mu\text{-}F(OsO_2F_3)_2^+$, SbF_5, SbF_6^-, $Sb_2F_{11}^-$, AsF_5, AsF_6^-, $[OsO_2F_3][SbF_6]$, and $[OsO_2F_3][Sb_2F_{11}]$ were calculated using density functional theory at the SVWN and B3LYP[62] levels. The Stuttgart semirelativistic large core and effective core pseudopotential basis sets (SDDall) augmented for F, O, and Sb with two d-type polarization functions by Huzinaga et al.[63] were used at the SVWN level, and the Stuttgart

(53) Gerken, M.; Dixon, D. A.; Schrobilgen, G. J. *Inorg. Chem.* **2000**, *39*, 4244–4255.
(54) *SMART*, version 5.611; *SAINT*, version 616.602; Siemens Energy and Automotive Analytical Instrumentation: Madison, WI, 1999.
(55) Sheldrick, G. M. *SADABS* (*Siemens Area Detector Absorption Corrections*), version 2.10; Siemens Analytical X-ray Instruments Inc.: Madison, WI, 2004.
(56) Sheldrick, G. M. *SHELXTL-Plus*, release 6.14; Siemens Analytical X-ray Instruments, Inc.; Madison, WI, 2000−2003.
(57) Farrugia, L. J. *J. Appl. Crystallogr.* **1999**, *32*, 837–838.
(58) *APEX2*, release 2.0−2; Bruker AXS Inc.: Madison, WI, 2005.
(59) *GADDS: General Area Detector Diffraction System*, V4.1.29: Smith, K. L., Jin, Z., Chambers, J. L., He, B., Preckwinkel, U., Moran, P. D., Eds.; Bruker: Madison, WI.
(60) Macrae, C. F.; Edgington, P. R.; McCabe, P.; Pidcock, E.; Shields, G. P.; Taylor, R.; Towler, M.; J., v. d. S.; Wood, P. A. *J. Appl. Crystallogr.* **2006**, *39*, 452–457.
(61) *TOPAS V2003: General Profile and Structure Analysis Software for Powder Diffraction Data - User's Manual*; Bruker AXS: Karlsruhe, Germany, 2005.
(62) Frisch, M. J. et al. *Gaussian 03*, revision B.04; Gaussian, Inc.; Pittsburgh, PA, 2003.
(63) Huzinaga, S.; Andzelm, J.; Kolobukowski, M.; Radzio-Andzelm, E.; Sakai, Y.; Tatewaki, H. *Gaussian Basis Sets for Molecular Calculations*; Physical Science Data 16; Elsevier: Amsterdam, 1984.

basis set augmented by one f-type polarization function (α_f Os 0.886)[64] for osmium and aug-cc-pVTZ basis sets for antimony, oxygen, and fluorine were used at the B3LYP level.

Pseudopotentials were used with the appropriate basis sets for both osmiun (SDDall-PP) and antimony (aug-cc-pVTZ-PP). The combined use of SDDall and SDDall-PP or aug-cc-pVTZ and aug-cc-pVTZ-PP basis sets are indicated as SDDall(-PP) or aug-cc-pVTZ(-PP). Quantum-chemical calculations were carried out using the programs Gaussian 98 and Gaussian 03.[65] The levels and basis sets were benchmarked by calculating the energy-minimized geometries and frequencies of *cis*-OsO_2F_4[16] and $Sb_2F_{11}^-$ and by comparison with the experimental values.[29,66] The geometries were fully optimized using analytical gradient methods. After optimization at one level of theory, the geometries were optimized at the other level of theory to ensure an equivalent energy-minimized geometry had been achieved. The vibrational frequencies were calculated at the SVWN and B3LYP levels using the appropriate minimized structure, and the vibrational mode descriptions were assigned with the aid of Gaussview.[67]

Acknowledgment. We thank the Natural Sciences and Engineering Research Council of Canada for the award of postgraduate scholarships (M.J.H.) and for support in the form of a Discovery Grant (G.J.S.) and SHARCNet (Shared Hierarchical Academic Research Computing Network; www.sharcnet.ca) for computational resources. We also thank Dr. James Britten, McMaster X-ray Facility, for his assistance in obtaining the variable-temperature X-ray powder diffraction data of $[OsO_2F_3][Sb_2F_{11}]$.

Supporting Information Available: View of $[OsO_2F_3][Sb_2F_{11}]$ crystallographic unit cell along the *c*-axis (Figure S1); calculated vibrational frequencies and assignments for $[OsO_2F_3][SbF_6]$ (Table S1); factor-group analyses for $[OsO_2F_3][Sb_2F_{11}]$ under the space groups $P\bar{1}$ and $P1$ (Table S2); X-ray powder diffraction patterns of $[OsO_2F_3][Sb_2F_{11}]$ at −150 and −173 °C (Figure S2); calculated geometrical parameters for $[OsO_2F_3][SbF_6]$ (Table S3 and Figure S3); natural bond orbital (NBO) valencies, bond orders, and NPA charges for $[OsO_2F_3][SbF_6]$ (Table S4); complete references 62 and 65; and X-ray crystallographic file in CIF format for the structure determination of $[OsO_2F_3][Sb_2F_{11}]$. This material is available free of charge via the Internet at http://pubs.acs.org.

(64) Ehlers, A. W.; Bohme, M.; Dapprich, S.; Gobbi, A.; Hollwarth, A.; Jonas, V.; Kohler, K. F.; Stegmann, R.; Veldkamp, A.; Frenking, G. *Chem. Phys. Lett.* **1993**, *208*, 111–114.

(65) Frisch, M. J. et al. *Gaussian 98*, revision A.11; Gaussian, Inc.: Pittsburgh, PA, 2003.

(66) Gillespie, R. J.; Landa, B.; Schrobilgen, G. J. *Inorg. Chem.* **1976**, *15*, 1256–1263.

(67) *GaussView*, release 3.0; Gaussian Inc.: Pittsburgh, PA, 2003.